Review Article

ADVANCED PHOTONICS

Advances in soliton microcomb generation

Weiqiang Wang,[a,†] Leiran Wang,[a,b,†] and Wenfu Zhang[a,b,*]

[a]Chinese Academy of Sciences, Xi'an Institute of Optics and Precision Mechanics, State Key Laboratory of Transient Optics and Photonics, Xi'an, China

[b]University of Chinese Academy of Sciences, Beijing, China

Abstract. Optical frequency combs, a revolutionary light source characterized by discrete and equally spaced frequencies, are usually regarded as a cornerstone for advanced frequency metrology, precision spectroscopy, high-speed communication, distance ranging, molecule detection, and many others. Due to the rapid development of micro/nanofabrication technology, breakthroughs in the quality factor of microresonators enable ultrahigh energy buildup inside cavities, which gives birth to microcavity-based frequency combs. In particular, the full coherent spectrum of the soliton microcomb (SMC) provides a route to low-noise ultrashort pulses with a repetition rate over two orders of magnitude higher than that of traditional mode-locking approaches. This enables lower power consumption and cost for a wide range of applications. This review summarizes recent achievements in SMCs, including the basic theory and physical model, as well as experimental techniques for single-soliton generation and various extraordinary soliton states (soliton crystals, Stokes solitons, breathers, molecules, cavity solitons, and dark solitons), with a perspective on their potential applications and remaining challenges.

Keywords: optical frequency comb; soliton microcomb; microcavity; photonic integration; Kerr effect; four-wave mixing.

Received Jan. 28, 2020; accepted for publication Apr. 23, 2020; published online Jun. 19, 2020.

[DOI: 10.1117/1.AP.2.3.034001]

1 Introduction

Optical microcavities, which emerged from the rapid development of modern micro/nanofabrication technologies, have grown to be revolutionary devices that light the way toward several fantastic applications, including advanced light sources, ultrafast optical signal processing, and ultrasensitive sensors, benefitting from their unprecedented small size and high buildup of energy inside the resonators.[1] The resonant optical field can be strongly enhanced in a high-quality (Q) factor microcavity, which results in long light–matter interaction lengths and ultralow thresholds for nonlinear optical effects.[2,3] In the case of microcavities made of materials with inversion symmetry (e.g., silica, silicon nitride, or crystals), the elemental nonlinear interaction is third-order nonlinearity, which gives rise to the parametric process of four-wave mixing (FWM). Together with the intrinsic filter character of microresonators, discrete optical frequency components with equal spacing can be generated, which are termed micro-optical frequency combs (μOFC or microcombs). Compared with traditional OFCs built on mode-locked solid-state or fiber lasers, microcomb is considered a new type of coherent light source that shows unique and promising advantages of lower power consumption as well as whole system integratability. Further, microcombs are also capable of generating ultrashort pulses with gigahertz to terahertz repetition rates,[4,5] which is far beyond the limitations of physical cavity length for conventional lasers; thus, they can find important applications in fundamental physical precision metrology.[6] Therefore, microcombs have been developed as a powerful alternative that enables miniaturization of OFCs and opens investigations into new nonlinear physics and corresponding applications.

Technically speaking, the character of microcomb mainly depends on microresonator properties as well as the pumping parameters (e.g., pump power and frequency detuning). The Q factor, dispersion profile, and cavity mode of a microresonator directly decide the threshold, bandwidth, and frequency spacing (and other related features) of emitted combs, respectively, while the pump settings determine the operation states and output performance such as the spectral envelope and noise characteristic. Since the landmark demonstration in 2003 of the

*Address all correspondence to Wenfu Zhang, E-mail: wfuzhang@opt.ac.cn

†These authors contributed equally to this work.

high-Q toroid microcavity with a Q-factor in excess of 100 million,[7] considerable efforts have been made to improve the Q of microcavities on various material platforms by developing fabrication techniques as well as more reliable approaches for generating broadband low-noise microcombs, as shown in Fig. 1. For example, Kippenberg et al.[2] obtained several discrete comb lines through optical parametric oscillation (OPO) in a silica toroid microcavity in 2004; thereafter, Del'Haye et al.[8] successfully achieved a microcomb covering ~500 nm in the telecom band in 2007. In 2011, Okawachi et al. [9] suggested that the noise of microcomb can be lowered through varying the pump detuning. One special mode-locked comb, termed a soliton microcomb (SMC), can be evolved from the primary comb and modulation instability (MI) comb while the pump sweeps across a resonance from the blue-to-red detuned regime.[10] Physically, solitons can be spontaneously organized in a continuous wave (CW)-driven microresonator, where double balances, nonlinearity and dispersion as well as dissipation and gain, are reached.[10] However, the states of microcombs are dependent on the pump-resonance detuning, where multiple operation possibilities exist for a resonator at a given pump power and frequency.[11] When the chaotic MI state transitions to the soliton state, the dramatic intracavity power drop can result in pump frequency shifting out of the cavity resonance through a thermo-optical effect, so achieving stable soliton operation is a great challenge in practical experiments. To overcome the strong thermal-optical effect that hinders steady SMC access, various schemes have been implemented. A representative work is the first temporal soliton generation using a frequency-scanning method;[10] since then "power-kicking,"[12,13] thermal tuning,[14] and auxiliary-laser-based[15,16] methods have been introduced. Meanwhile, rich types of soliton states, including Stokes soliton induced by the Raman effect,[17] dual-soliton generation in a single microcavity,[18] soliton crystals,[19] breathers,[20] laser cavity solitons,[21] soliton molecules,[22] and dark pulse states operating in a normal-dispersion regime,[23] have all been discovered (Fig. 1). And a variety of nonlinear phenomena (e.g., dispersive wave, mode crossing, and Raman self-frequency shift) that are closely related to the characteristics of microresonators have also been disclosed.[12,24–27] All of these achievements suggest that SMCs can establish an interface between soliton physics and integrated photonics as well as materials science.

Until now, based on advanced experimental techniques, SMCs have been realized in an MgF_2 whispering-gallery-mode (WGM) resonator,[10] silica disk[13] and microrod,[28,29] AlN,[30] $LiNbO_3$,[31] and CMOS-compatible microring resonator of SiN,[12] Si,[32] and high-index doped silica glass.[15] Table 1 briefly summarizes some typical SMCs obtained on various material platforms with distinct cavity properties. Furthermore, because of the developed fabrication process and improved-dispersion engineering, SMCs with different spectral coverages have been demonstrated on various material platforms. As shown in Fig. 2, SMC generation in the visible,[31,33] near-,[10,13,15,30,34,35] and mid-infrared[36] regions have all been achieved, covering a wavelength range of down to ~750 nm[31] and up to ~4300 nm.[36] Benefitting from the full coherent feature across the whole spectral coverage[10–12,37] the advent of SMCs has promoted research in various applications, such as dual-comb spectroscopy (DCS),[38] terabit coherent optical communications,[39] photonic-integrated frequency synthesizers,[40] ultrafast distance measurements,[41] and calibration of astrophysical spectrometers for exoplanet searching.[42] Beyond these developed applications, SMCs are also relevant to a large variety of physical systems that could provide ideal testbeds for fundamental theory of nonlinear wave dynamics research.[43,44]

In this review, we summarize recent experimental achievements with a perspective on the potential and challenges. The remainder of this paper is organized as follows. Sec. 2 introduces the basic theory and physical model of microcomb generation. In Sec. 3, we mainly focus on the presented techniques for single SMC generation, including the rapid frequency and thermal tuning, power-kicking, forward and backward sweeping, auxiliary-laser-assistance, self-injection-locking using CW lasers, and synchronous driving by pulsed sources.

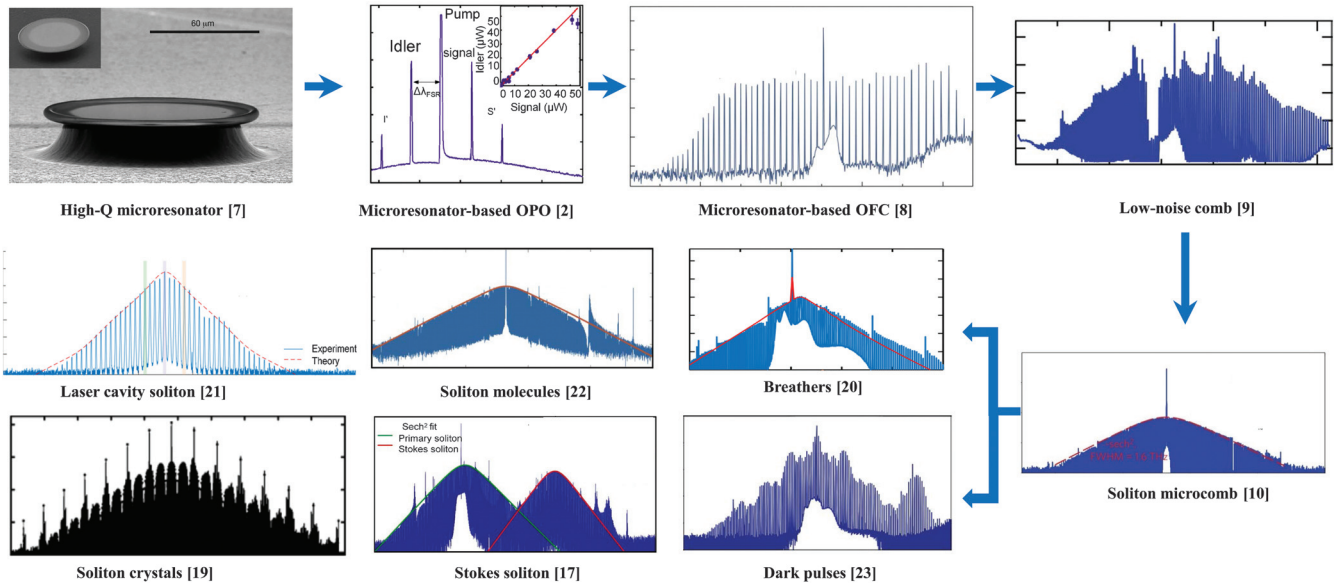

Fig. 1 Route map of microcombs.

Table 1 Typical parameters of reported SMCs.

Material	Structure	Q	FSR (GHz)	Wavelength range (nm)	Types	Refs.
MgF_2	Rod	4.3×10^8	35.2	1520 to 1590	Solitons	10
MgF_2	Rod	$>1.0\times10^8$	14	1520 to 1590	Solitons	24
MgF_2	Rod	$\sim4.7\times10^8$	25.78	1540 to 1580	Solitons	36
MgF_2	Rod	$>10^9$	12.5	1526 to 1548	Solitons	45
SiO_2	Disk	$\sim4\times10^8$	22	1510 to 1600	Solitons	13
SiO_2	Disk	$\sim10^8$	~20	1025 to 1125 and 760 to 790	Solitons	33
SiO_2	Disk	$>10^8$	22	1600 to 1650	Stokes solitons	17
SiO_2	Disk	$>10^8$	1.8 to 33	1530 to 1570	Solitons	4
SiO_2	Disk	$>10^8$	26, 16.4	1540 to 1580	Soliton crystals	46
SiO_2	Disk	1.8×10^8	22	1510 to 1590	Solitons	47
SiO_2	Rod	$>10^8$	55.6	1520 to 1590	Solitons	28
SiO_2	Rod	3.7×10^8	50	1530 to 1590	Solitons	29
AlN	Ring	0.65×10^8	>500	1400 to 1700	Solitons	30
SiN	Ring	$\sim5\times10^5$	189	1330 to 2000	Solitons	12
SiN	Ring	$\sim0.4\times10^5$	1000	1100 to 2300	Solitons	48
SiN	Ring	1.4×10^6	1000	1420 to 1700	Solitons	49
SiN	Ring	$\sim0.6\times10^6$	1000	850 to 2000	Solitons	34
SiN	Ring	$\sim0.5\times10^6$	200	1440 to 1660	Solitons	50
SiN	Ring	$>2.0\times10^6$	200	1470 to 1620	Breathers	51
SiN	Ring	$\sim1.9\times10^6$	>200	1450 to 1700	Breathers	20
SiN	Ring	$\sim8.0\times10^6$	194	1540 to 1640	Solitons	52
SiN	Ring	$>15\times10^6$	99	1570 to 1630	Solitons	53
SiN	Ring	$\sim0.65\times10^6$	~1000	776 to 1630	Solitons	35
SiN	Ring	$\sim0.77\times10^6$	231.3	1460 to 1610	Dark pulses	23
Doped silica glass	Ring	$\sim1.7\times10^6$	49	1480 to 1650	Solitons	15
Doped silica glass	Ring	$\sim1.7\times10^6$	49	1480 to 1650	Soliton crystals	19
Doped silica glass	Ring	$\sim1.3\times10^6$	49	1510 to 1580	Cavity solitons	21
Graphene-nitride	Ring	$\sim10^6$	~90	Tunable[a]	Soliton crystals	54
Silicon	Ring	0.2×10^6	127	2800 to 3800	Breathers	51
$LiNbO_3$	Ring	2.2×10^6	199.7	750 to 800 and 1460 to 1650	Solitons	31
$LiNbO_3$	Ring	$>1.1\times10^6$	~200	1830 to 2130	Solitons	55

Note: All results are approximate values obtained from the reported literature.
[a]Spectral coverage of 1450 to 1700 nm was experimentally verified in Ref. 54.

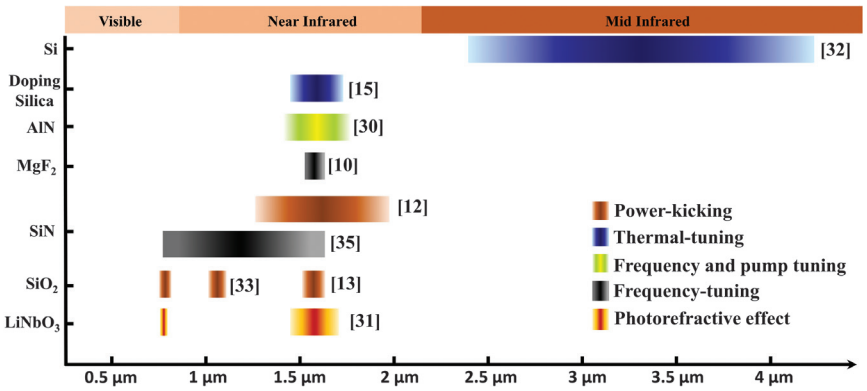

Fig. 2 Typical spectral coverage of SMCs on various material platforms using different approaches.

Various extraordinary soliton states, including soliton crystals, Stokes solitons, breathers, soliton molecules, laser cavity solitons, and dark pulses, are discussed in Sec. 4. Finally, in Sec. 5, a brief summary of the valuable applications of SMCs is given, and an outlook on the underlying challenges and opportunities for this field is presented in Sec. 6.

2 Physics and Numerical Models for Microcombs

The generation of microcombs arises from parametric frequency conversion through the FWM effect that generates a pair of photons (a signal and an idler) that are equally spaced to the pump. The photonic interaction can be expressed as $2\hbar\omega_p \rightarrow \hbar\omega_s + \hbar\omega_i$, where ω_p, ω_s, and ω_i are the pump, signal, and idler angular frequencies, respectively. The frequencies of the newly generated photons are resonance enhanced in microcavity resonances $\omega_{s,i} = \omega_p \pm n\Delta\Omega$, where $\Delta\Omega$ is the angular frequency of the free-spectral-range (FSR) that is determined by the cavity optical length and $n = 1, 2, \ldots$ is the mode number with the assumption of the pump at mode 0. For theoretical description of the microcomb formation mechanism, firstly the evolution of each mode amplitude A_μ can be modeled using a nonlinear wave equation. Then the microcomb generation process can be completely described by a set of autonomous, nonlinear, and coupled ordinary differential equations, which are called coupled mode equations (CMEs):[56,57]

$$\begin{aligned} \dot{A}_\mu &= -\frac{\kappa}{2}A_\mu + \delta_{\mu 0}\sqrt{\eta\kappa}s_{\text{in}}e^{-i(\omega_p-\omega_0)t} \\ &\quad + ig\sum_{\mu'\mu''\mu'''} A_{\mu'}A_{\mu''}A^*_{\mu'''}e^{-i(\omega_{\mu'}+\omega_{\mu''}-\omega_{\mu'''}-\omega_\mu)t} \\ s_{\text{out}} &= s_{\text{in}} - \sqrt{\eta\kappa}\sum A_\mu e^{-i(\omega_\mu-\omega_p)t}, \end{aligned} \tag{1}$$

where κ is the cavity decay rate, including the intrinsic and coupling decay rate. $\eta = \kappa_{\text{ext}}/\kappa$ is coupling efficiency, $|s_{\text{in,out}}| = \sqrt{P_{\text{in,out}}/\hbar\omega_0}$ denote the amplitudes of the pump and output powers. $\delta_{\mu 0}$ is the Kronecker's delta. For microcomb formation, $\delta_{\mu 0}$ equals 1 for the pump mode and 0 for other modes. The nonlinear coupling coefficient $g = (\hbar\omega_0^2 c n_2)/(n_0^2 V_{\text{eff}})$ describes the cubic nonlinear gain, where n_0 and n_2 are the refractive index and nonlinear refractive index, respectively, V_{eff} is the effective cavity volume, and c and $\hbar$ are the speed of light and the Planck constant, respectively. The resonant frequencies ω_μ of a microcavity can be Taylor-expanded around the pump mode as

$$\omega_\mu = \omega_0 + D_1\mu + \frac{1}{2}D_2\mu^2 + \frac{1}{6}D_3\mu^3 + \cdots, \tag{2}$$

where ω_0 is the angular frequency of the pump mode, also regarded as the reference frequency. μ is the relative mode number of the resonance away from the reference frequency. $D_1/2\pi$ is the FSR of the resonator at the frequency ω_0. D_2 and D_3 are the second- and third-dispersion parameters, respectively. $\omega_p - \omega_0$ represents the pump detuning, where ω_p is the pump frequency. The summation includes all μ', μ'', μ''' respecting the relation $\mu = \mu' + \mu'' - \mu'''$. The above model assumes that the power density of all modes are spatially overlapped.

The CMEs have been successfully used to determine the threshold and explain the role of dispersion as well as other mechanisms in the microcomb formation. However, the amount of computation increases dramatically with increases in the mode number. Through considering the total intracavity field an entirety $A(\theta, t) = \sum_\mu A_\mu(t)e^{i\mu\theta}$, where $\theta \in [-\pi, \pi]$ is the azimuthal angle along the resonator, the CMEs can be simplified to the equivalent approach of the Lugiato–Lefever equation (LLE), which is also referred to as the spatiotemporal model:[58–60]

$$\frac{\partial A}{\partial t} = \sqrt{\kappa_{ex}}S_{\text{in}} - \left(\frac{\kappa}{2} + i2\pi\delta\right)A + \sum_{k=2}^{n} i^{k+1}\frac{\zeta_k}{k!}\frac{\partial^k A}{\partial\theta^k} + ig|A|^2A, \tag{3}$$

where ζ_k represents the dispersion parameters. The LLE can be optimally solved using the split-step Fourier algorithm considering the periodic boundary conditions of microresonators.

Based on the LLE, mode-locked microcombs have been predicted and rich physical phenomena have been explained, including the single soliton with dispersion wave,[12] soliton crystals by taking into account of perturbation,[46] and dark pulse states with a modified form to involve mode interaction.[23] Raman self-frequency shift was also precisely simulated by adding the Raman response item $f_R h_R \otimes |A|^2$ to the LLE, where f_R indicates the Raman fraction and h_R is the Raman response function.[25,27]

3 Experimental Schemes for Single SMC Generation

It has been found that SMC can be spontaneously formed while a CW pump stabilizes in the red-detuned regime of a dissipative nonlinear microcavity. However, the soliton existing range exhibits thermal instability for microcavities with negative temperature coefficients, which blinded SMC observation for more than 6 years since the first microcomb realization.[8,10] Therefore, the major challenge for SMC generation has been how to stabilize a pump in the red-detuned regime of a microcavity. An intuitive thought is preventing the cavity from heating up before the pump sweeping to the soliton existing range, such as the frequency scanning method for SMC realization in a low thermal-optic coefficient MgF_2 microcavity.[10] Since then several equivalent and more universal schemes have been developed, e.g., the power-kicking, thermal tuning, and self-injecting locking methods. Another solution for SMC generation is realizing the intracavity thermal balance using an auxiliary laser to maintain the intracavity optical power. Taking advantage of the smooth spectral envelope and fixed temporal spacing, single SMC is the most desired soliton state for applications, which gives rise to great research interest for deterministic single SMC generation, wherein the backward frequency/temperature scanning and pulse-pumped schemes have been introduced. In this section, we will focus on the experimental progress of single SMC generation.

3.1 Frequency-Scanning Method

The basic idea of the frequency-scanning method is sweeping the pump to the red-detuned regime before the microcavity is heated up by the thermo-optic effect. Generally, the frequency-scanning speed is determined by the thermo-optic response time, Q-factor, as well as the pump power.[10,25,44,61–63] This method is first introduced for SMC generation in an MgF_2 microresonator. The experimental setup is shown in Fig. 3(a).[10] A tunable

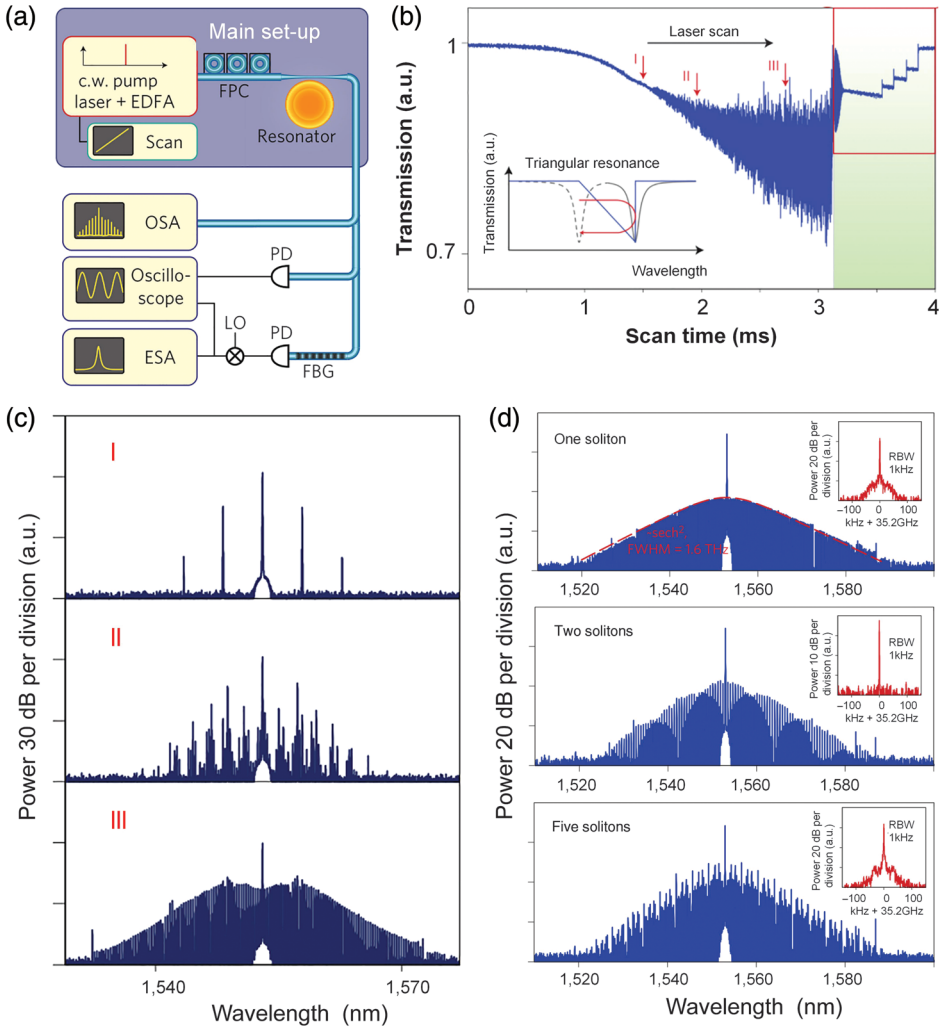

Fig. 3 Experimental demonstration of stable temporal solitons in a high-Q MgF_2 microresonator using the frequency-scanning method. (a) Experimental setup for stable temporal soliton generation. (b) Optical transmission power trace when the pump scans over a resonance. The discrete steps in the red-detuned regime (green shading) indicate existence of cavity solitons. (c) Optical spectral evolution while the pump sweeps in the blue-detuned regime. (d) Optical spectra for SMCs with 1, 2, and 5 solitons. OSA, optical spectrum analyzer; ESA, electrical spectrum analyzer; PD, photodetector; LO, local oscillator; FPC, fiber polarization controller; EDFA, erbium-doped fiber amplifier. Images are adapted with permission from Ref. 10.

narrow-linewidth laser is used as the pump with its frequency sweeping speed and scanning range controlled by an electrical signal. The soliton existing range shows regional thermal stability due to the self-phase and cross-phase modulation (XPM) induced nonlinear phase shift. Therefore, the intracavity thermal equilibrium can be reached when the pump sweeps to the red-detuned regime with an appropriate speed, which leads to SMC generation and maintenance. Figure 3(b) presents the transmission power trace when the pump scans over one cavity resonance. Before the pump reaches the zero-detuning point, the intracavity optical field first evolves from the primary comb (I) to the subcomb (II) and then to the MI comb (III) state in succession; the corresponding optical spectra are shown in Fig. 3(c). Once the pump transmits into the red-detuned regime, the intracavity power suffers a sudden decline and exhibits transmission steps that indicate the generation of SMCs. Figure 3(d) presents the optical spectra for one-, two-, and five-soliton states. Since the SMCs are fully coherent, the corresponding beat notes exhibit sharp frequency lines [insets of Fig. 3(d)], reflecting excellent low-noise characteristics.

The pump frequency-scanning method is a fundamental and intuitional approach for SMC generation. The success of this method relies on the control of the pump frequency sweeping speed and accuracy. The laser scanning time should be comparable to the cavity lifetime and thermal lifetime of the microresonator, which has a very high Q and relatively large thermal volume. Meanwhile, the laser wavelength should exactly stabilize at the soliton steps. Because of the limited tuning speed and the frequency accuracy or stability of tunable lasers, it is a challenge for single SMC generation in microresonators with short thermal lifetimes.[63] To improve the applicability of the frequency-scanning method, a single-sideband suppressed-carrier

(SSB-SC) frequency shifter is introduced to improve the frequency tuning speed as well as the frequency control accuracy, which is determined by the driven radio-frequency signal. Using an SSB-SC as a frequency shifter, SMCs have been realized in Si_3N_4 and AlN microresonators with soliton steps lengths on the order of tens to hundreds of nanoseconds.[30,47]

For some special cases, SMCs can also be generated with relatively slow scanning speeds once the thermal dynamics during soliton formation can be stabilized by other approaches. For example, a partial overlapping mode can be used to compensate for the thermal dissipation when the pump tunes to the red-detuning regime. By taking advantage of an adjacent mode family in a specific Si_3N_4 microring, the thermal challenge is overcome for stable SMC generation.[48] Additionally, through scanning the pump to a fixed frequency, delayed spontaneous soliton generation from the chaotic state is also observed, which is tuning speed independent.[49]

3.2 Power-Kicking Scheme

For microresonators with a high thermal-optic effect, the durations of soliton steps are so short that stopping the laser frequency exactly within these steps is technically difficult.[63] As shown in Figs. 4(c)–4(e), the typical durations of soliton steps are on the order of submicroseconds for Si_3N_4 microresonators. It becomes a great challenge to stabilize the pump in such short soliton steps considering the performance of practical tunable lasers. A more universal solution is using modulators to control the pump power and timing sequence stringently, which is termed the power-kicking approach.[12]

A typical experimental setup is shown in Fig. 4(a). More details concerning this technique are depicted in Fig. 5, where the pump laser passes through an electro-optic modulator (EOM), an EDFA, and an acousto-optic modulator (AOM) before coupling to a Si_3N_4 microresonator.[63] First, the AOM lowers the pump power before the laser tunes into the resonance and increases the pump power within soliton steps at the end of the thermal triangle of the resonance. Second, a fast pump power drop modulated by EOM is introduced before the pump sweeps across the zero-detuning point. The fast power drop reduces the nonlinear thermal and induces a fast zero-detuning transition of the pump laser. Accordingly, the pump power, modulation depth, and initial timing should be carefully optimized for stable SMC generation.[63] Examples of the timing sequence of the pump frequency sweeping, fast EOM modulation, and slow AOM modulation are shown in Figs. 5(b)–5(e). Such a "power-kicking" method has proved to be capable of achieving reliable transition into soliton state, and solitons with over 2/3 octave bandwidth were observed [Fig. 4(f)] benefitting from the soliton-induced Cherenkov radiation.[12]

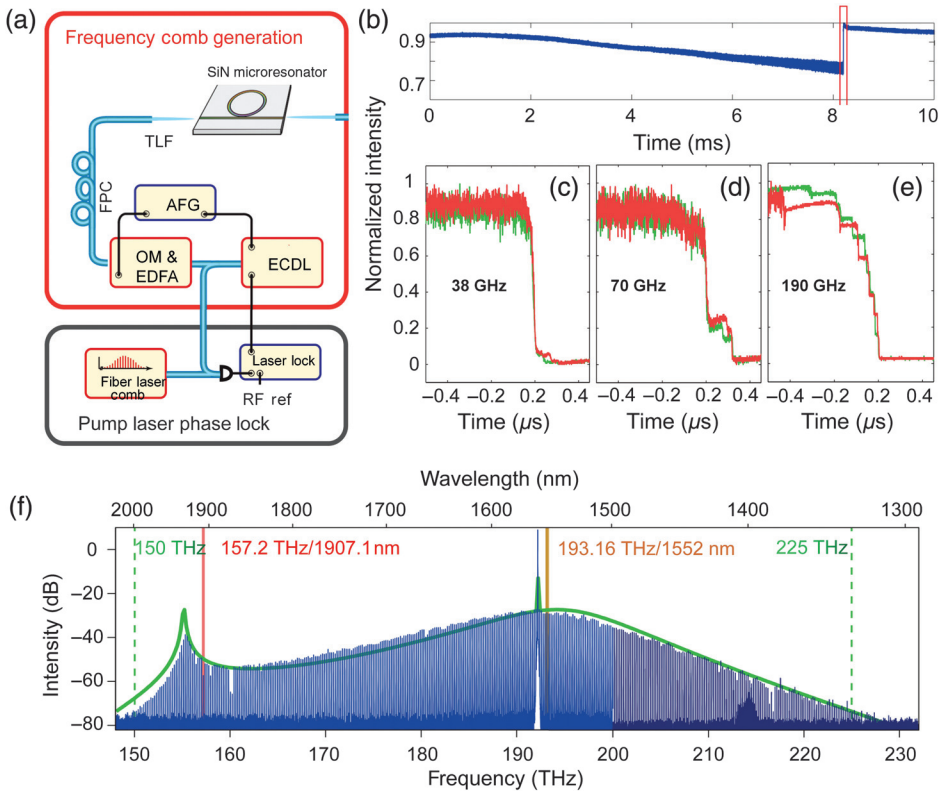

Fig. 4 SMC generation based on power-kicking scheme. (a) Experimental setup of power-kicking scheme. The microresonator is pumped by an external cavity diode laser that is amplified and modulated by an AOM and an EOM. (b) Typical triangular shape of the transmission power while the pump sweeps across a resonance. (c)–(e) Soliton steps of Si_3N_4 microcavities with repetition rates of 38, 70, and 190 GHz, respectively. (f) Measured optical spectrum of single SMC covering over 2/3 octave bandwidth. AFG, arbitrary function generator; EDFA, erbium-doped fiber amplifier; FPC, fiber polarization controller; OM, optical modulator; RF, radio frequency; TLF, tapered-lensed fiber. Images are adapted with permission from Ref. 12.

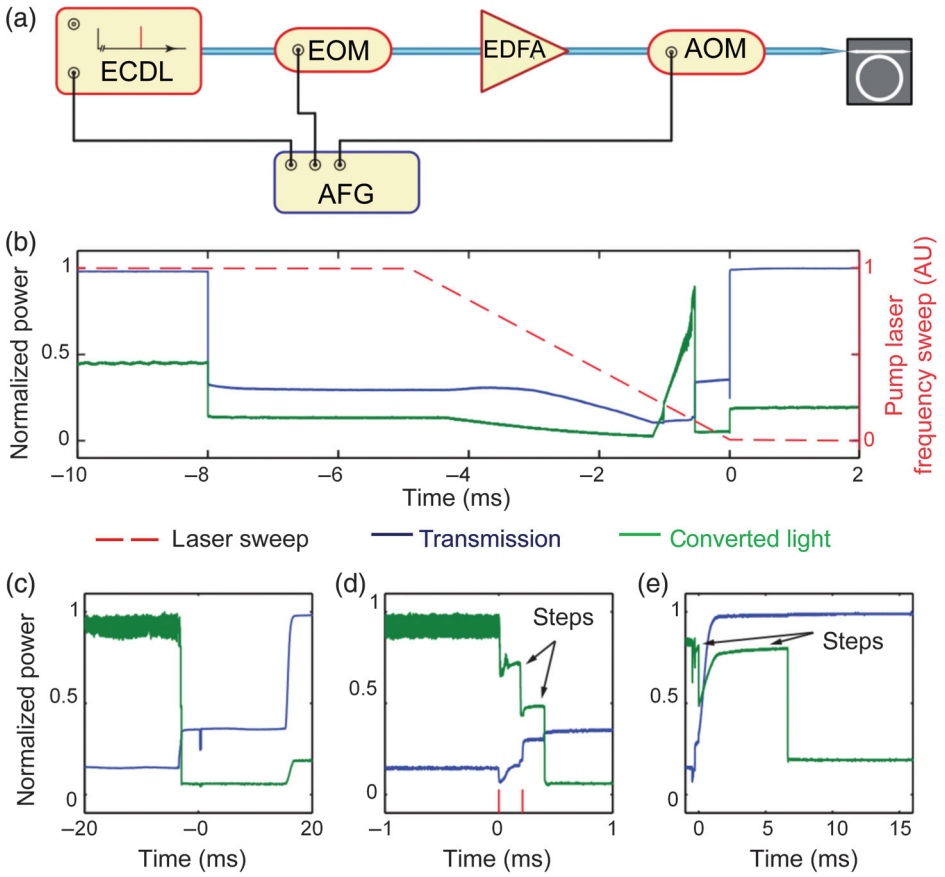

Fig. 5 Schematic and timing sequences of the power-kicking scheme. (a) Setup used to bring very short-lived soliton states to a steady state, including two modulators to adjust the pump power. (b) Timing sequences of the pump scanning, the fast and slow power modulation, and the converted light power. (c) Initial timing of the fast modulation with respect to the thermal triangle and slow power modulation. (d) The fast power modulation induced soliton steps. (e) Combined effect of the fast and slow modulation. Images are adapted with permission from Ref. 63.

For cases with long enough soliton steps (e.g., longer than several microseconds), a single AOM can provide enough modulation speed for SMC generation. Additionally, the pump parameters can be adjusted with an active feedback loop to realize active capture and stabilization of temporal solitons.[64] The power-kicking scheme has been widely used in some proof-of-concept applications such as DCS[38] and microcomb-based range measurement.[65] However, additional modulators and the precision control circuit complicate the SMC system, which increases the technical difficulties for miniaturized integration. Therefore, more compact SMC generation approaches, such as the thermal-tuning method and self-injected locked scheme, have been developed and are discussed next.

3.3 Thermal-Tuning Method

An equivalent approach for SMC generation is shifting the resonances of a microresonator through a thermal-tuning method rather than tuning the pump frequency. As shown in Fig. 6, a narrow-linewidth laser with a fixed frequency is used as the pump, and the microcavity resonances are thermally controlled by an on-chip heater.[14] Through controlling the heater current, the cavity resonances can shift at a sufficiently high speed that is induced by changing the waveguide refractive index due to the thermo-optic effect. Along with the current reducing (temperature decreasing), one resonance passes through the pump and characteristic soliton steps can be observed as shown in Fig. 6(b). Although the lifetime of these soliton steps is on the order of microseconds, SMCs can still be obtained because of the high control accuracy of the heater current tuning speed and stop value.

In principle, the thermal-tuning method can be regarded as a variant of the pump frequency-scanning method. Compared with tunable lasers, fixed frequency lasers usually have much narrower linewidth and lower noise. So it is attractive for soliton generation using a fixed frequency laser to improve the microcomb performance. Meanwhile, a fixed frequency laser has a smaller footprint and the integration technique of current source is rather mature, so the thermal-tuning method has the potential to realize a fully integrated microcomb.[52]

3.4 Auxiliary-Laser-Based Method

Because the challenges of SMC generation mainly arise from the thermal instability of the soliton existing range, it is reasonable to imagine that the thermal effect can be solved by maintaining

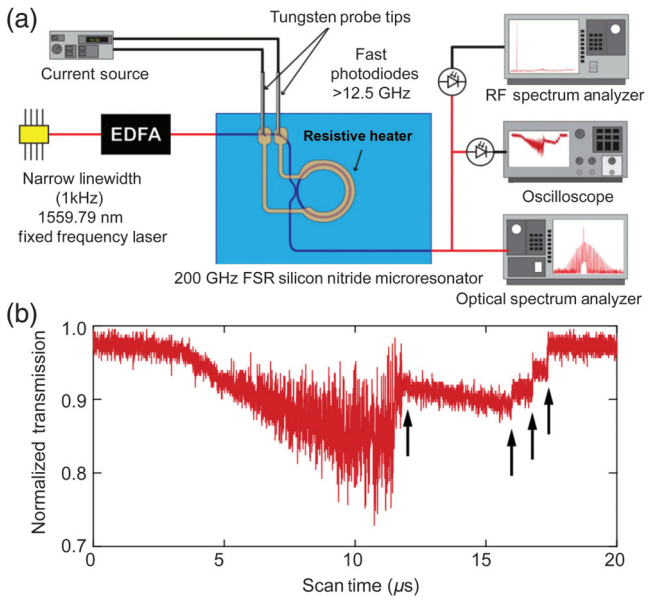

Fig. 6 SMC generation based on thermal-tuning method. (a) Experimental setup of thermally controlled SMC generation in a Si_3N_4 microresonator. (b) Transmission optical power trace of the generated microcomb. Steps marked by arrows indicate transitions between different multisoliton states. Images are adapted with permission from Ref. 14.

the intracavity optical power at a similar level during SMC generation. It is noted that microresonators exhibit contrary thermal characters when pumps are located at the blue- and red-detuned regimes. As a result, the dramatic decrease of intracavity heat when a pump laser tunes into a soliton existing range can be effectively compensated for by an auxiliary laser located at the blue-detuned regime. This principle has been verified recently,[15,16,28,29,34] and the requirement for a rigid tuning time (on the order of thermal lifetime) can be relaxed using the auxiliary-laser-assisted approach.

A typical experimental setup is shown in Fig. 7(a), where the auxiliary and pump lasers are counter-coupled into a Si_3N_4 microresonator.[16] Figure 7(b) shows the relative position of resonances and lasers during the tuning process. First, the auxiliary laser is settled at the blue-detuned side, which approaches the resonance peak. Then the pump is tuned into another resonance from the counter-propagating direction. Once the pump laser enters the red-detuned regime, the intracavity power drop can be compensated for by the auxiliary laser and the cavity resonance could be stabilized. Therefore, transition from the chaotic comb to soliton states can be stably realized, and the tuning process is no longer dependent on the tuning speed. As shown in Fig. 7(c), during the soliton generation process, the total intracavity power remains at a similar level, which avoids the resonance drifting.

Based on the auxiliary-laser-assistant thermal-balance approach, a new SMC regime is discovered in which the soliton power exhibits a negative slope versus pump frequency detuning. It is distinct from the traditional soliton existence regime with a positive slope that is accessible via thermal locking by thermal-avoided methods. The negative slope implies that the increase of average comb power is less than the decrease of pump background, resulting in the total intracavity power decreasing with the increasing of detuning. In another experiment, it is proved that the durations of soliton steps can be extended by two orders of magnitude under the assistance of a codirectional-coupled 1.3-μm auxiliary laser, enabling robust soliton generation by even

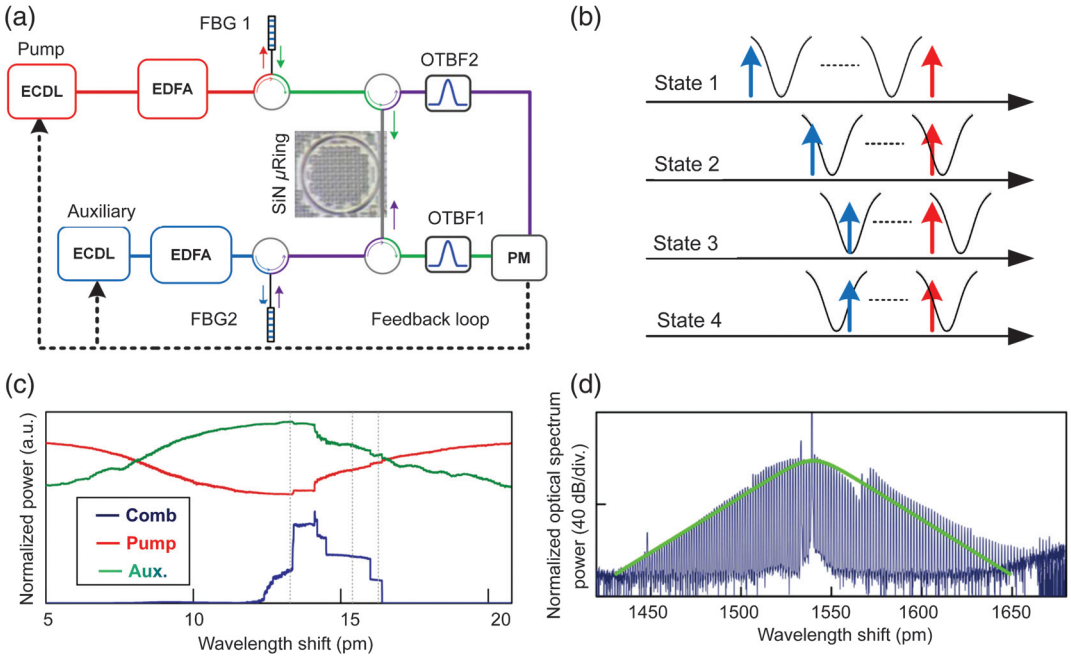

Fig. 7 SMC generation by the auxiliary-laser-based method. (a) Experimental setup. (b) Schematic of the counter-coupled auxiliary-laser-assisted thermal response control method. (c) The pump and auxiliary laser counter-balance thermal influences on the microcavity. (d) Optical spectrum of single SMC. Images are adapted with permission from Refs. 16 and 66.

manual tuning of the pump frequency into resonance with sub-milliwatt-level power.[29] Besides, SMCs are also realized in silica and high-index doped silica glass microresonators.[15,28]

All of these experimental results suggest that using an auxiliary laser can contribute to intracavity thermal equilibrium. It is regarded as an effective and universal method for stable SMC generation. Further, the auxiliary laser provides an additional degree of freedom for microcomb dynamic research. For example, the frequency spacing of the auxiliary and pump lasers has a significant impact on the microcomb states, and the beating between the auxiliary and pump lasers provides an optical lattice for soliton capture, which would be helpful for soliton crystal generation. This method can also provide a feasible approach to realizing spectral extension and synchronization of a microcomb in a single microresonator.[67]

3.5 Photorefractive Effect for Stable SMC Generation

Because of the negative temperature coefficient of microresonators, the soliton existing range exhibits thermal instability, which results in complex pump tuning techniques for SMC generation. By contrast, if the refractive index of a microresonator decreases with increasing intracavity optical power, the pump can enter the red-detuned regime stably for SMC generation, just like the MI comb generation in a negative temperature coefficient microresonator. It has been discovered that the photorefractive effect in a Z-cut $LiNbO_3$ waveguide can cause an intensity-dependent decrease in the refractive index.[31] Moreover, the photorefractive effect has a stronger influence on the refractive index compared with that of the thermo-optic effect, which results in the red-detuned regime becoming a thermal stable region.[31]

Figure 8(a) schematically shows the influence of the photorefractive effect, which is opposite to that induced by the thermo-optic nonlinearity. The inset of Fig. 8(a) presents the measured transmission power trace while a laser passes through a resonance from the red-detuned side. It is found that the response time of the photorefractive effect is much slower than that of the thermo-optic effect. Accordingly, if the tuning speed of the pump frequency is faster than the response time of the photorefractive effect, the microresonator is first affected by the thermo-optic effect, which causes resonance red-shift and induces intracavity power increase. Therefore, three different dynamic processes may take place depending on the pump frequency tuning speed. When the pump scanning time is less than the thermal lifetime, the thermo-optic effect will dominate and no SMC can be stabilized. Once the pump scanning time is comparable to the thermal lifetime, power spikes will be

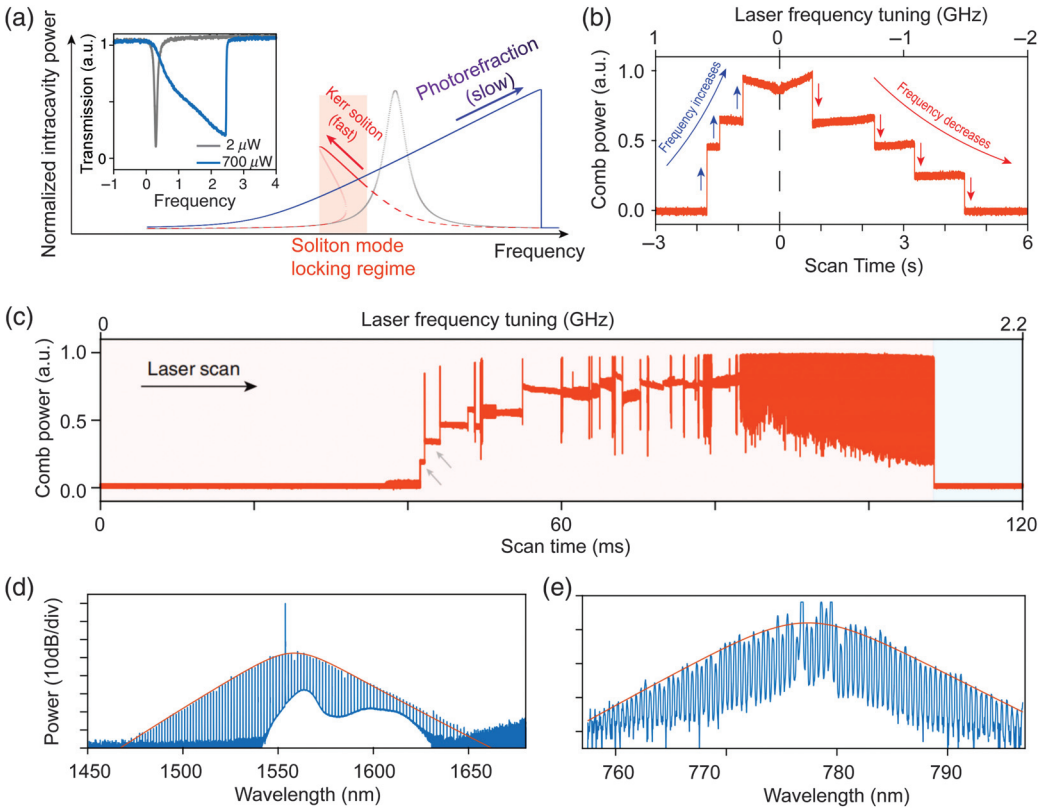

Fig. 8 Bichromatic SMC generation in a $LiNbO_3$ microresonator. (a) Schematic for influences of optical Kerr and photorefraction effects. The inset is the measured optical power traces when a pump sweeps across a resonance from the red-detuned side. (b) Comb power trace versus scanning time when the pump slowly sweeps forward and backward in the red-detuned regime. (c) Comb power trace versus scanning time when the pump rapidly sweeps from the red- to blue-detuned regimes. The power spikes are caused by the relatively slower response speed of the photorefraction effect. (d) and (e) Optical spectra of SMCs in near-infrared and visible bands, respectively. Images are adapted with permission from Ref. 31.

observable as shown in Fig. 8(c). If the pump scanning speed further decreases, the power spikes can be effectively suppressed as shown in Fig. 8(b).

Because of the photorefractive effect, the thermal instability of the soliton existing range is completely compensated for. Therefore, SMC can be stably generated by coupling a pump into the resonance from the red-detuned side, and the pump can freely tune forward and backward for soliton switching. Meanwhile, the thermal stability of the soliton existing range can contribute to simplification of control circuits for SMC generation, which is crucial for miniaturized integration and practical applications. More interestingly, the $LiNbO_3$ waveguide has not only the Kerr effect but also second-order nonlinearity, which results in visible SMC generation by the second harmonic effect. It is an effective approach to realizing bichromatic microcombs when the cavity material has second- and third-orders nonlinearity simultaneously, which has also been verified in aluminum nitride microresonators.[68] The second harmonic effect provides another approach for SMC generation in the visible frequency band where microcavities suffer from higher transmission loss.

3.6 Forward and Backward Tuning Method

Due to the inherently stochastic intracavity dynamics, it remains a challenge to realize repeatable soliton switching and deterministic single SMC generation if using the aforementioned strategies. For example, Fig. 9(b) shows the overlap optical power traces once the pump laser sweeps over a microresonator resonance using the forward frequency-tuning method. It clearly demonstrates that the soliton number N is random, with a high probability of $N = 6$ (predominantly), 7, 8, or 9.[69] In addition, the step duration decreases with decreasing N, indicating that the single SMC is not reliably accessible using only the forward-tuning technique.

After the frequency-scanning method was proposed, a forward and backward frequency-sweeping technique was introduced for deterministic single SMC generation.[69] Briefly, the forward frequency tuning is first applied for multiple-SMC generation. In the next stage, the pump sweeps backward with a slow scanning speed, leading to successive reduction of the soliton number. The cavity dynamics comparison of forward and backward frequency tuning methods is shown in Figs. 9(a)–9(d). Physically,

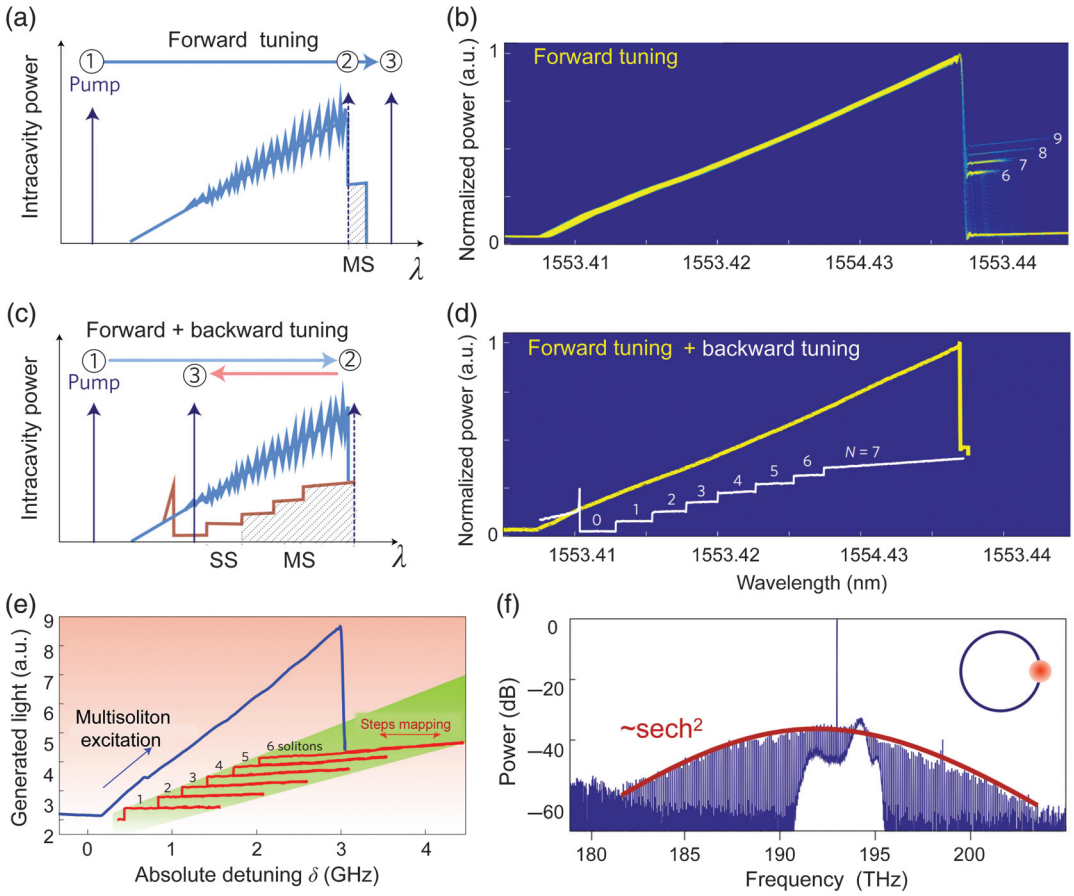

Fig. 9 (a) Scheme of the forward frequency-tuning method. (b) 200 overlaid experimental traces of the output comb light in the pump forward tuning, revealing the formation of a predominant soliton number of $N = 6$. (c) Scheme of the laser forward and backward tuning. (d) Experimental traces of the forward tuning (in yellow) and backward tuning (in white) for soliton switching and deterministic single SMC generation. (e) Measured absolute soliton existing range of a Si_3N_4 microring. The lower boundary δ_L presents staircase pattern that can be stably accessed step by step using backward-scanning method. (f) Optical spectrum of single SMC in a 100-GHz Si_3N_4 microresonator. Images are adapted with permission from Ref. 69.

it has been revealed that the soliton-switching process depends on the character of a soliton existence range ($\delta_L < \delta < \delta_H$, where δ_L and δ_H are the lower and higher boundaries of the soliton existence range, respectively). Figure 9(e) shows the measured absolute soliton existence range with different soliton numbers in a Si_3N_4 microresonator. With the decrease of the soliton number, the resonances are blue-shifted to reduce the intracavity energy, and the absolute detuning of the pump reveals a staircase pattern. The microcomb power will "jump" down the staircase steps when the pump sweeps backward; by contrast, the microcomb power drops dramatically and SMC annihilates directly when the pump continues sweeping forward. So the backward tuning technique can help to reliably access the single SMC state starting from an arbitrary multisoliton state. The backward tuning process must be adiabatic for successive soliton annihilation, i.e., thermal equilibrium is satisfied at every soliton annihilation step. Therefore, the backward scanning speed has to be much slower than the thermal relaxation rate of the microresonator. Figure 9(f) exhibits the single SMC when the pump backward sweeps at a speed of ~40 MHz/s, while the forward tuning speed is ~100 GHz/s.

A parallel progress on deterministic single SMC generation was fulfilled in a high-index doped silica glass microring through the forward and backward thermal-tuning method.[15] The high-Q microcavity is butterfly packaged with a thermoelectric cooler, which contributes to convenient manipulation of the cavity temperature. An orthogonally polarized auxiliary laser is used to balance the intracavity thermal effect, which introduces a tuning speed independent of the soliton state generation. Throughout the experiments, the wavelengths of the pump and auxiliary lasers are fixed once chosen. Similarly, the multisoliton state is first obtained through decreasing the operation temperature, and then the temperature is backward-tuned for deterministic single SMC generation. The corresponding power traces for the comb light and the auxiliary laser are shown in Figs. 10(a) and 10(b), where each step represents one- or multisoliton annihilation. Figure 10(c) presents the measured optical spectra of SMCs. The forward and backward tuning method provides a feasible approach toward a program-controlled autogeneration of single SMC.

3.7 Self-Injection Locking

One of the ultimate goals for the microcomb field is fully integrated SMC sources. A common feature of all methods mentioned above is reliance on external narrow-linewidth pumps, which introduces great challenge for miniaturized integration. Benefitting from the advanced micro/nanofabrication technologies, ultra-high-Q resonators can pave the way toward soliton sources directly driven by an ordinary semiconductor laser. Recently, self-injection locking methods were demonstrated by combining an MgF_2 WGM resonator and a Fabry–Pérot laser diode (FP-LD).[45] Figure 11(a) shows the schematic of self-injection locking in an MgF_2 WGM resonator. The high-Q microresonator plays double roles. First, it acts as an external cavity to select the LD lasing mode and narrow the linewidth via the self-injection locking effect.[70,71] Second, it is used as a nonlinear low-threshold Kerr medium for soliton generation. Figures 11(b)–11(d) depict the processes of self-injection locking and SMC generation. The system can be smoothly switched into a soliton regime by tuning the FP-LD driven current. Because the back-reflection time is shorter than the thermal relaxation time, the laser frequency follows the thermally shifted cavity resonance, which suppresses the thermal instability in real time.[45] As a result, the thermal instability problem can be effectively solved, which results in tuning speed independence. Therefore, this method could eliminate the requirement

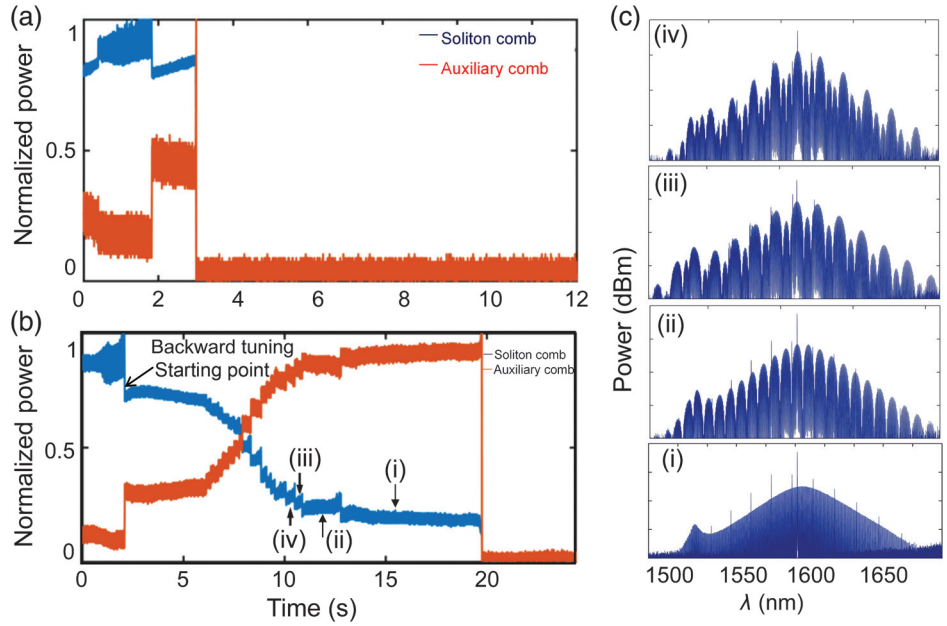

Fig. 10 Deterministic single SMC generation using thermal-tuning method.[15] (a) Power traces when just decreasing the operation temperature. (b) Power traces using forward and backward operation temperature tuning method. (c) Optical spectra for soliton number of 4, 3, 2, and 1 in a 49-GHz high-index doped silica glass microring. Images are adapted with permission from Ref. 15.

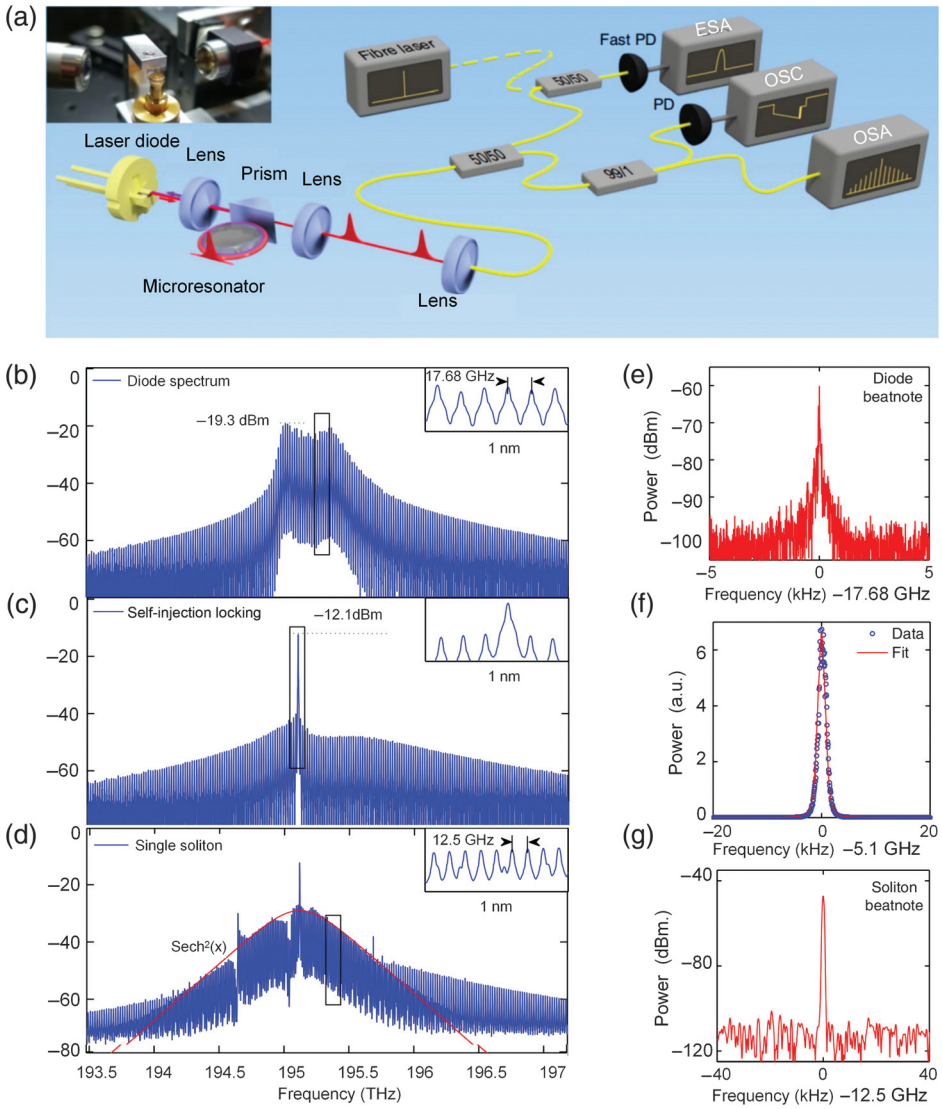

Fig. 11 Self-injection locking and spectral narrowing of a multifrequency laser diode coupled to an MgF_2 ultrahigh-Q WGM microresonator. (a) Experimental setup. (b)–(d) Spectrum and (e)–(g) the corresponding beat note signal for the free-running multifrequency diode laser, laser stabilized by the microcavity, and single SMC in the self-injection locking regime, respectively.[45]

of special techniques for delicate amplitude or frequency manipulation.[10,63,64,69]

A key factor of this technique is the Q of the microresonator, which not only improves the backscattering light for pump frequency-locking but also lowers the needed pump power for SMC generation. Along with the success of on-chip ultra-high-Q microresonator fabrication, a series of achievements on directly pumped soliton generation have been realized.[72–75] For example, one achievement utilizing this scheme is directly butt-coupling an FP-LD chip (InP) to a high-Q Si_3N_4 microcavity.[72] Through tuning the drive current of the FP-LD, the laser is first switched to single-mode lasing; then MI comb, breather soliton, and single soliton are realized consecutively. Very recently, the Q factor of a Si_3N_4 microcavity has been successfully boosted to 1.6×10^7 with the improved fabrication process, and a butterfly packaged SMC source at a radio frequency rate of 15 GHz is realized.[74] The employed self-injection locking scheme also shows a unique feature of permitting soliton generation through binary turn-on and turn-off of the pump laser, which results in the "turnkey" operation without additional photonic/electronic control circuits. Another investigation shows that Kerr nonlinearity can significantly modify the locking dynamics by red-shifting the laser emission frequency, where self-phase modulation and XPM of the clockwise and counter-clockwise light enable soliton formation.[75] All of this progress suggests that the self-injection locking approach has proved to be a practical and competitive technique in the development of microcombs, benefiting from eliminated requirements for complex tuning schemes or feedback loops for soliton generation and stabilization, as well as relieved power consumption introduced by redundant electronic components. Until now, because of the limited lasing power of integrated pump lasers, the bandwidth of these integrated SMCs has been limited to tens of nanometers. It is believed that microcombs with a broader bandwidth and higher power will be reached with the realization of more powerful LDs in near future. The self-injected locking method offers a new route toward combining

integrated microresonators and chip-scale lasers to establish an ultracompact electrically driven SMC system.

3.8 Pulse-Pumped Single-Soliton Generation

In addition to the narrow-linewidth CW lasers, temporally structured light sources can also be used as a pump for SMC generation.[11,76,77] The merits of pulse-pumped schemes are reduction of the pump power and improvement in the conversion efficiency. Meanwhile, the generated soliton pulses are copropagating with pump pulses, which results in the synchronization of repetition rates. The principle for this scheme is depicted in Figs. 12(a) and 12(b). The CW-driven soliton is supported by the resonantly enhanced CW background, while for pulse-driven case SMC can form only when the inverse driving pulse repetition rate matches the soliton roundtrip time.[76] This process is akin to but different from the conventional OPO systems that also utilize a synchronous pump. The pump pulses act as optical lattices for solitons capture, which results in the generated stable femtosecond dissipative solitons locating "on top" of the driving pulses. In the first pulse-pumped SMC generation experiment, an EOM-based picosecond pulse generator was used as the pump source. Both the repetition rate (f_{rep}) and carrier-envelope-offset frequency (f_{ceo}) of pump pulses are directly controlled via tuning the RF frequency and CW laser frequency, respectively. As shown in Fig. 12(c), when the central driving mode is scanned across a resonance from blue- to red-detuning like the frequency-tuning method, the resonator transmission shows characteristic soliton step features. The step can sustain for a wide spanning interval of f_{rep} [Fig. 12(d)], indicating that precise control of the driving pulse repetition rate is not strongly required for the SMC formation in a pulsed pump system.

Following the pulse-pumped cavity soliton generation in fiber and Fabry–Pérot cavities,[78,79] generation has also been realized in a chip-based SiN microring, which can provide a spurious-free spectrum of resolvable calibration lines in the demonstration of a proof-of-concept microphotonic astrocomb.[77] Importantly, locking cavity solitons to the external driving pulse (or soliton self-synchronization) enables direct, all-optical control of both the repetition rate and carrier-envelope offset frequency for the microcomb. Through stabilizing the subharmonically (i.e., the soliton repetition rate is twice that of the EOM frequency) driven astrocomb to a frequency standard, the absolute calibration with a precision of 25 $cm\,s^{-1}$ is successfully achieved.[77] Further, through locking one microcomb mode to an atomic transition, absolute optical-frequency fluctuations at the kilohertz level over a few seconds and <1-MHz day-to-day have been achieved recently.[80]

Physically, a pulse pump can break the symmetry of a microcavity, which induces optical lattice for soliton capture. The soliton quantity is determined by the repetition rate, width of the pump pulse, and intrinsic properties of the microresonator (dispersion, Q-factor, etc.). Therefore, SMCs with a deterministic repetition rate can be realized through controlling the pump repetition rate and pulse width. Until now, the repetition rate of a pulse-pumped SMC is still limited to the bandwidth of EOM. Actually, repetition-rate-multiplicable SMCs can also be realized using harmonic or rational harmonic driving

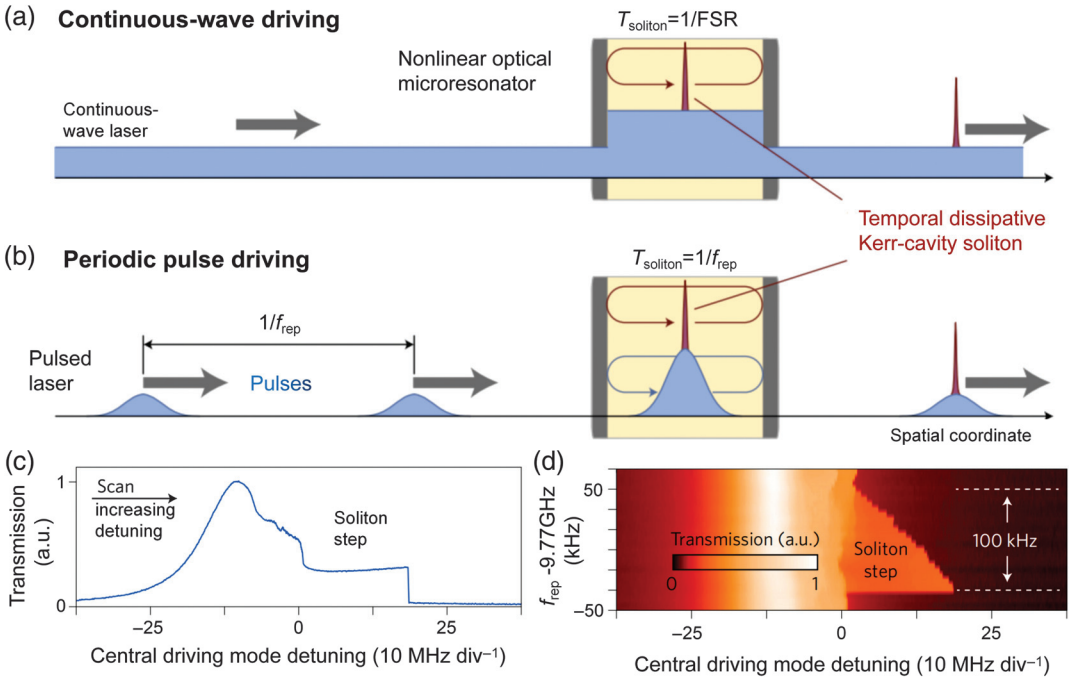

Fig. 12 Principle and experimental scheme for SMC generation driven by optical pulses.[76] (a) For the CW-driven case, solitons propagate with a resonantly enhanced CW background. (b) For the pulse-driven case, pump pulses with repetition rate f_{rep} periodically drive the solitons. (c) Resonator transmission trace as the central driving mode scans across a resonance for an optimized repetition rate. (d) Contour plot of the resonator transmission showing soliton steps can exist for a wide (100 kHz) spanning interval of f_{rep}. Images are adapted with permission from Ref. 76.

pulses,[81] which is beneficial by improving the energy conversion efficiency and flexibility of SMCs.

4 Extraordinary Soliton Microcombs

Different soliton forms in microcavities besides typical single or multisolitons, such as the soliton crystals, Stokes solitons, breather solitons, soliton molecules, laser cavity solitons, and dark pulses (solitons), also exist. They present distinct behaviors in both frequency and time domains, as well as enrich soliton dynamics and physics for microcomb research. In this section, the generation of these extraordinary solitons and their unique characteristics are reviewed.

4.1 Soliton Crystals

Soliton crystals defined as spontaneously and collectively ordered ensembles of copropagating solitons that are regularly distributed in a microcavity were recently discovered in silica WGM,[46] Si_3N_4,[54,82] high-index doped silica glass,[19] and $LiNbO_3$[83] microresonators. The generation of soliton crystals is found to be related to the extended background wave, which is formed by the beating between the mode with excess power caused by mode crossing and the pump laser. Copropagating solitons interact with each other and "crystallize" by arranging themselves into a self-organized sequence.[46] Theoretically, the energy of all steady solitons circulating in a given microresonator is expected to be quantized to a certain value, which is determined by the resonator properties, pump power, and detuning. This phenomenon can be understood as the discrete steps found in the transmission power trace while sweeping the pump across a resonance.[19] Therefore, the intracavity power will linearly increase with the soliton number. Once there are enough solitons coexisting in a microresonator, the total intracavity energy would approach a similar level to that of a chaotic MI state. The typical soliton crystals step appears at the peak of the transmission power trace and exhibits excellent thermal stability. The intracavity temperature fluctuation is relatively small and has little effect on the resonance frequency, so soliton crystals can be stably formed using slow tuning techniques without complex techniques to overcome the thermo-optic effect. For example, the soliton crystal generation is almost independent of the thermal or pump frequency tuning speed, even allowing manual tuning with a second-level response time. Figure 13 shows the representative optical spectral and temporal characters of soliton crystals obtained in a silica disk[46] and a high-index doped silica glass microresonator.[19] Because of the strong interactions between the dense soliton ensembles, soliton crystals exhibit unique "palm-like" spectra, which are the superposition of the "primary-like" and the underlying soliton spectrum. There are different soliton arrangements that induce a rich variety of soliton crystal states, such as the perfect state [Fig. 13(I a)], Schottky defects with vacancies [Figs. 13(I b)–13(I e) and 13(II a)–13(II i)], Frenkel defects [Figs. 13(I f)–13(I i) and 13(II j)], disorder [Fig. 13(I j)], superstructure [Figs. 13(I k)–13(I n) and 13(II k)], and irregular intersoliton spacings [Figs. 13(I o) and 13(II l)]. In another experiment, soliton crystals with Schottky defects are also

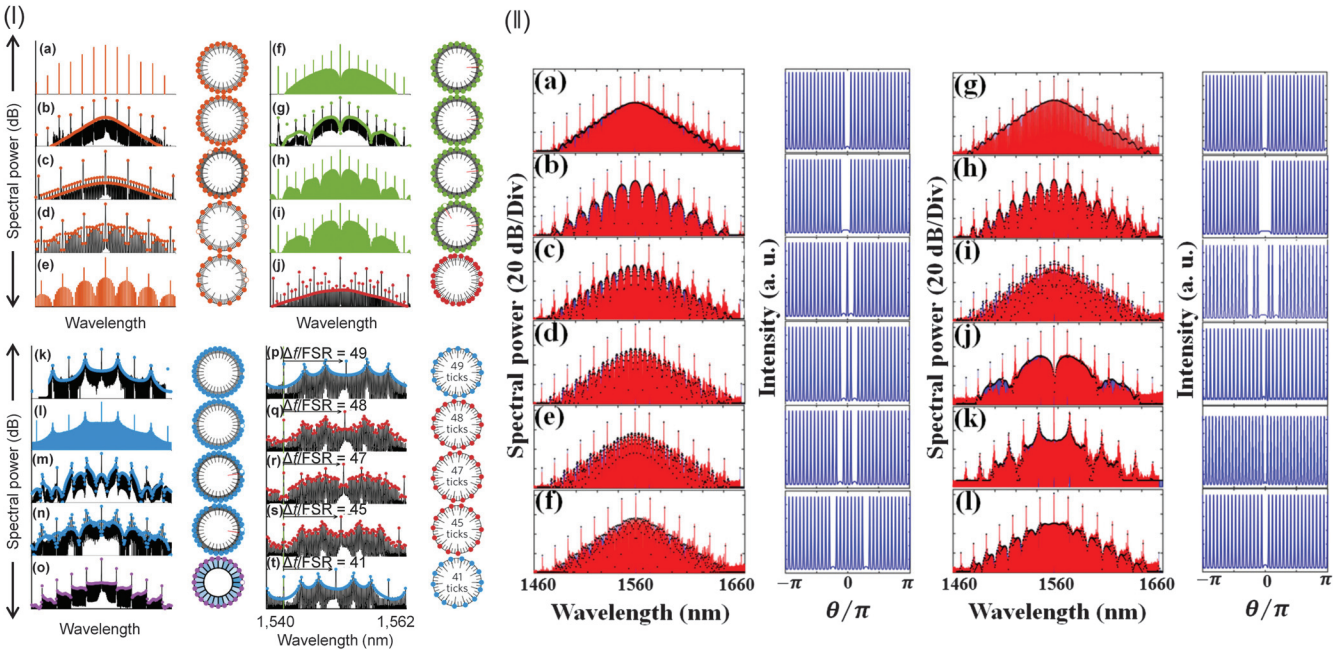

Fig. 13 (I) Soliton crystals in a silica disk resonator.[46] Left panel: measured (in black) and simulated (in color) optical spectra. Right panel: schematic depictions of the corresponding soliton distribution in the resonator with major ticks indicating (expected) soliton location and minor ticks indicating peaks of extended background wave due to mode crossing. (II) Soliton crystals in a high-index doped silica glass microring.[19] Left panel: measured (in red) and simulated (blue solid circles) optical spectra. Right panel: simulated temporal traces exhibiting (expected) soliton distributions of the corresponding soliton crystals. Images are adapted with permission from Refs. 19 and 46.

observed in a graphene-nitride microresonator, where the cavity dispersion becomes adjustable and affects the spectral bandwidth and shape.[54]

A special state of soliton crystals, i.e., the perfect soliton crystals (PSCs), is defined as all solitons are evenly distributed in a cavity and experimentally observed recently.[82,83] In a certain sense, such PSCs could be regarded as single SMC in a microresonator with larger FSR and thus, be capable of boosting the repetition rate to beyond THz level and breaking the limitation of bending loss for extremely small microresonators. Meanwhile, compared with single SMC in a same microresonator, the power of each comb line is multiplied by $N \times N$ times and energy conversion efficiency by N times (N for soliton number of PSCs). It is also found that, if the intracavity thermal influence is overcame, realization of PSCs with arbitrary soliton number becomes possible by adjusting the pump frequency to periodically change the background waves.[83]

Soliton crystals introduce a new regime of soliton physics and act as a test bed for the research of soliton interaction. The extreme degeneracy of the configuration space of soliton crystals suggests its capability in on-chip optical buffers.[46] Meanwhile, benefitting from a tiny intracavity energy change, the easy accessibility and excellent stability of soliton crystals could facilitate SMCs toward a portable and adjustable system for out of laboratory applications.

4.2 Stokes Soliton

Stokes soliton is a special type of soliton that arises from Kerr-effect trapping and Raman amplification when a first soliton (primary soliton) is present.[17] Figure 14(a) shows the principle of Stokes soliton, with its spectrum located in the Raman gain range and the repetition rate autolocked to the primary comb through Kerr-phase modulation. Considering the dispersion of microcavities, the Stokes soliton occupies a different mode family, which has a similar FSR at the Raman gain band. The FSRs of different transverse mode families of a silica microdisk cavity are shown in Fig. 14(b). It clearly shows that the Stokes soliton mode at a wavelength of 1593 nm has a near-identical FSR with the primary soliton mode at the pump wavelength of 1550 nm.[17] In the experiment, primary soliton is first excited using the power-kicking method. As the Stokes soliton originates from the Raman effect, which has a threshold power to obtain sufficient Raman gain to overcome round-trip loss, once the Stokes soliton is generated, the primary soliton power is clamped to a steady value and the Stokes soliton power is increased beyond the primary soliton power. A typical spectrum of the Stokes soliton is shown in Fig. 14(d); its central wavelength is 1593 nm, which is consistent with the mode analysis. The inset of Fig. 14(d) shows the high-resolution spectrum, which confirms a different mode is used for Stokes soliton generation. The

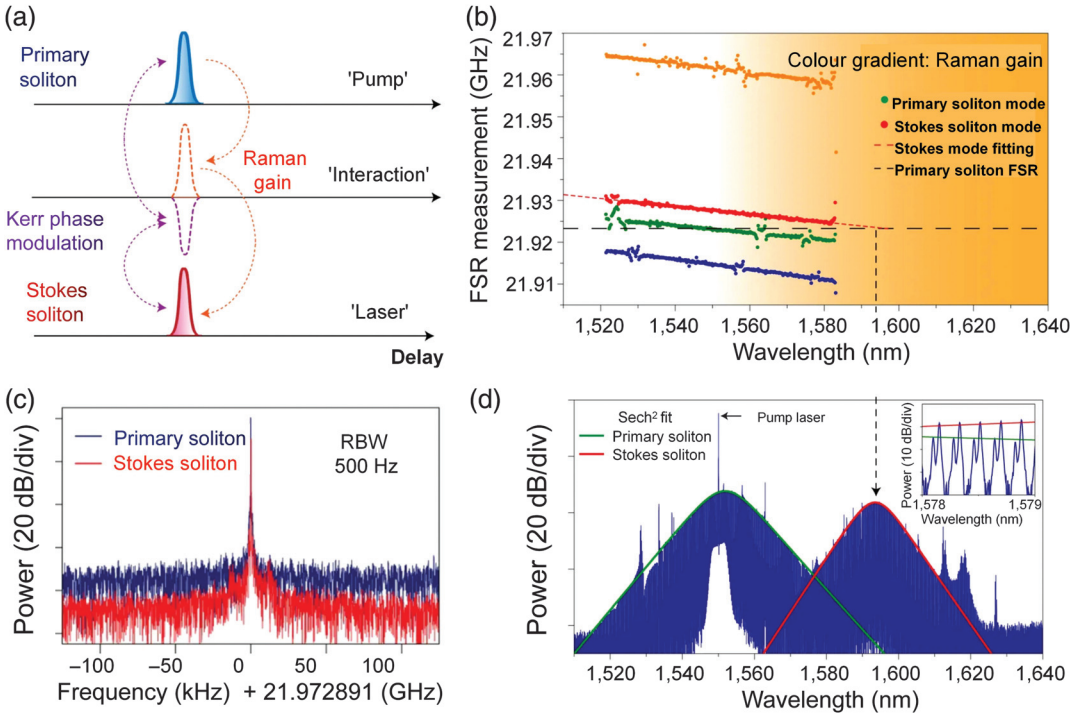

Fig. 14 Stokes soliton in a high-Q silica microdisk.[17] (a) Stokes soliton (red) is overlapped with primary soliton (blue) in time and space, which introduces maximum Raman gain. Stokes soliton is trapped by optical potential well induced by Kerr effect, which locks the repetition rate to the primary soliton. (b) Measured FSRs of different mode families versus wavelength of a 3-mm silica microdisk cavity. (c) Beating RF spectra of isolated Stokes and primary soliton, indicating the repetition rate of Stokes soliton is locked to primary comb. (d) Measured optical spectrum of Stokes soliton. The inset shows the high-resolution spectrum of the overlapping range, which confirms that the Stokes soliton is formed in a different mode family. Images are adapted with permission from Ref. 17.

measured RF spectra of the isolated primary and Stokes solitons are shown in Fig. 14(c), where the beating spectra are aligned, which verify the automatching of repetition rates of the Stokes soliton and primary soliton.

The central wavelength of the Stokes soliton relies on the FSR matching of distinct mode families, which offers a potential approach for controllable multicolor soliton generation through advanced-dispersion engineering techniques.[84] Thus, it contributes to the SMC generation even in the spectrum range where anomalous-dispersion or high-power pump is not achievable.

4.3 Breather Solitons

Distinct from the stationary soliton states mentioned above, breather solitons show periodic oscillation in both pulse amplitude and duration[20,51,85–87] as schematically shown in Figs. 15(a) and 15(b). Physically, breather solitons are nonlinear waves in which the energy is localized in space but oscillates in time (or vice versa), which has been found in various subfields of natural science.[88,89] To date, breather solitons have been observed in different material platforms, including Si_3N_4,[20,51,85,88] MgF_2 crystalline,[85,88] and Si[51] microresonators. The typical operation regime and accessing method of breather solitons are illustrated in Fig. 15(c), whereas the simulated transmission power trace versus pump detuning is depicted in Fig. 15(d). It can be clearly seen that the breather soliton regime is between the unstable MI and steady soliton regimes,[51] and breather solitons are generated with a relatively small pump detuning range. Therefore, an additional step is usually required for breather soliton generation. That is, first tune the laser to excite stable solitons as usual (e.g., via forward frequency scanning), and then, importantly, tune the pump laser backward together with increasing the pump power for the realization of breather solitons [Fig. 15(c)]. Note that this process is similar to but different from the forward and backward tuning method mentioned above, where the backward-tuning process is a necessary adiabatic step for deterministic single SMC generation. Compared with stationary solitons, the spectra of breather solitons are characterized by a sharp top and a quasitriangular envelope (on logarithmic scale) [Fig. 15(e)] instead of the sech^2-like profile, resulting from the averaging of the oscillating comb bandwidth by an optical spectrum analyzer. Meanwhile, for the RF spectra, breather solitons are identified by sharp tones that indicate oscillation at a low frequency (the fundamental breathing frequency and its harmonics) rather than a single one at the cavity repetition rate, suggesting the low-noise feature of the stationary soliton state [Fig. 15(f)].

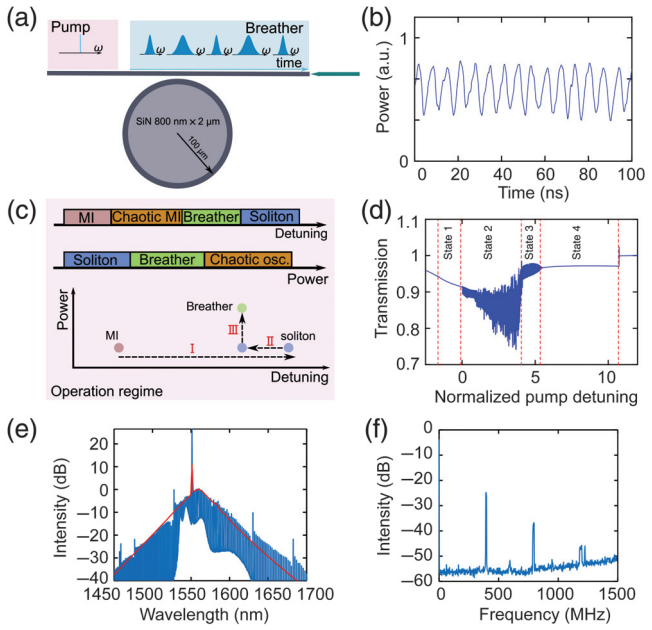

Fig. 15 Breather soliton in a Si_3N_4 microresonator. (a) Schematic of soliton "breathing" behavior in a microcavity. (b) Recorded power trace of breather solitons. (c) Operating regimes of microcombs. Breathers are generated at relatively small detuning and high pump power through three steps (illustrated by I, II, and III). (d) Simulated transmission power trace. States 1 to 4 correspond to the primary comb, unstable MI, breather solitons, and stationary soliton state, respectively. (e) Averaged spectrum of the breather soliton in a Si_3N_4 microresonator. (f) RF spectrum of breather soliton. Images are adapted with permission from Refs. 20 and 51.

The breather soliton state also can be triggered by avoided mode crossings (regarded as the intermode breather soliton), which is a ubiquitous phenomenon in multimode microresonators as illustrated in Figs. 16(a) and 16(b).[85] Usually, in the absence of intermode interactions, solitons in microcavities exist within a continuous range of the laser detuning where the soliton power smoothly evolves over the change of detuning. At the lower boundary of the soliton existing range [yellow shaded area in Fig. 16(a)], there is an intrinsic breathing state that has an oscillatory power trace, corresponding to the normal breather soliton existence range. When the intermode interaction is taken into account, a different breathing dynamic can be clearly seen in Fig. 16(b), which increases amplitude jitter close to the bistability region in the power trace. To observe intermode breather solitons, a single cavity soliton is first obtained; then continuously tuning the pump frequency within the soliton existing range, at a specific pump detuning, the intermode breather soliton can be excited, which is indicated in the form of sidebands on the RF beat note (breathing frequency). As this kind of breather soliton derives from the intermode interaction, the breathing mode generally has a narrow bandwidth, which results in the intermode breather soliton having an overall sech^2-shape spectral envelope (similar to the stationary SMCs) in the primary mode family but featuring several spikes (i.e., enhanced power in comb teeth) due to the phase matching to the cavity soliton,[85] as shown in Figs. 16(c) and 16(d). So this breathing behavior can be understood as being associated with a periodic energy exchange between the solitons and a second optical mode family. As a consequence, the discovery of widely existing breather solitons significantly enriches the dissipative soliton phenomena in a microresonator, as well as contributes to understanding the soliton dynamics within the larger context of nonlinear optics.

4.4 Soliton Molecules

Soliton molecules are balanced states in which attractive force caused by group velocity dispersion (GVD) of bound solitons is counteracted by the intersoliton repulsive force induced by the XPM effect.[22] Figure 17(a) shows the principle of the balance of attractive and repulsive forces between distinct solitons. When a microresonator is driven by discrete pumps [Fig. 17(c)], solitons with different pulse energies can form once the pumps

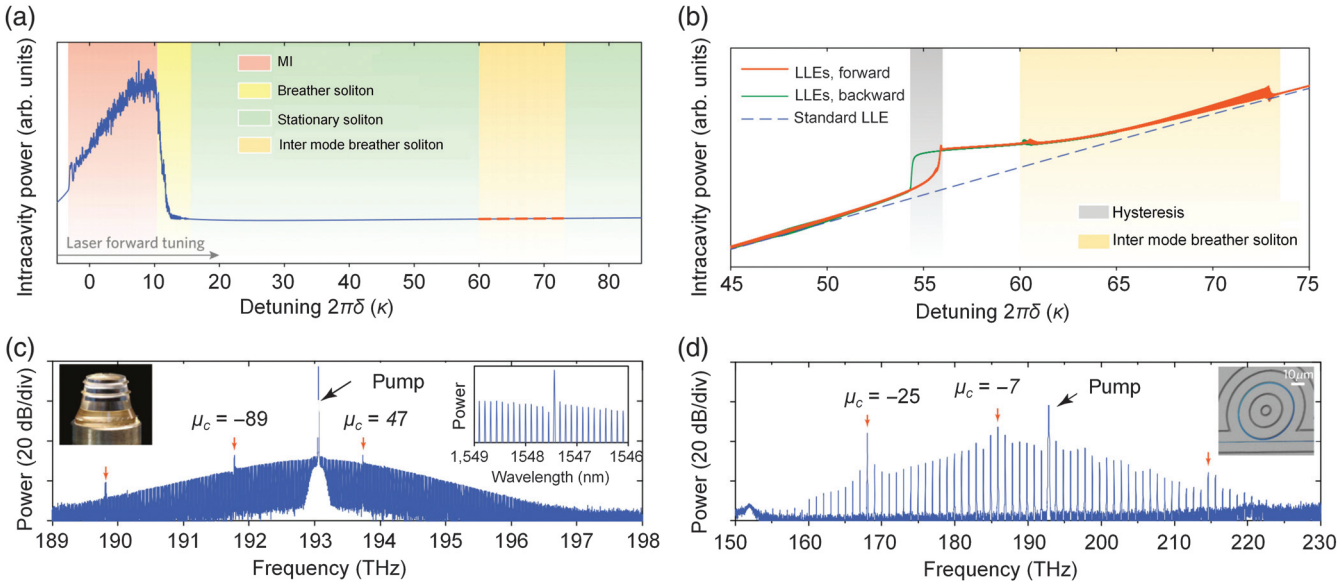

Fig. 16 Intermode breather solitons in microcavities. (a) Simulated intracavity power trace over the laser detuning in the absence of intermode interactions. The intermode breather soliton exists in the region where stationary soliton is expected (orange area). (b) Simulated power trace based on the coupled LLEs, showing a hysteretic power transition (gray area) and an oscillatory behavior (orange area). (c), (d) Measured optical spectra for intermode breather solitons in (c) an MgF_2 crystalline microresonator and (d) a SiN microring, which exhibits spikes that result from intermode interactions. Images are adapted with permission from Ref. 85.

are stabilized in the red-detuned regime simultaneously. The relationship of repulsive force (drifts of the distinct solitons) versus the soliton temporal gap can be calculated by

$$\frac{\mathrm{d}\tau}{\mathrm{d}t} = -\frac{1}{A_s}\,\mathrm{Im}\int \frac{\partial E_s^*}{\partial \tau} E_b\,\mathrm{d}\tau, \tag{4}$$

where A_s is the major soliton amplitude, E_s and E_b are the major soliton and the background fields including both of the minor soliton and beating background wave. The calculated result is shown in Fig. 17(b). It is observed that the repulsive force appears when the intersoliton separation is <300 fs. Therefore, when the distinct solitons have a large temporal gap, the attractive force plays a leading role and solitons get close to each other until the attractive force is balanced by the repulsive force.

Concerning experimental realization, discrete pumps are obtained by modulating a CW laser using an EOM. The frequency separation of discrete pumps is controlled by the driven RF signal. An example work is implemented in an MgF_2 WGM resonator with a loaded-Q of 1×10^9, as shown in Fig. 17.[22] When the pumps rapidly sweep across a resonance, the recorded transmission power trace, shown in Fig. 17(d), is characterized by the double MI comb to SMC transitions. The red-shaded area is the power trace of the major microcomb, which has higher power and a broader bandwidth, and the optical spectrum for single SMC is shown in Fig. 17(f). Figure 17(g) shows the optical spectrum of minor soliton, which has a narrower spectrum bandwidth, and the transmission power trace is presented by the blue-shaded area in Fig. 17(d). Once these two solitons are bound with each other, the optical spectrum is the linear superposition as shown in Fig. 17(e). The temporal separation of bound soliton is about 500 to 800 fs, which is of the same order of individual soliton pulse width, indicating that a balance is established between the attractive and repulsive forces, resulting in the same propagation velocity in the cavity.

Soliton molecules in microcavities go beyond the frame of their predecessors in fiber lasers, which enriches the soliton physics. In terms of applications, soliton molecules might contribute to comb-based sensing and metrology by providing an additional coherent comb, as well as optical telecommunications if storing and buffering soliton-molecule-based data come true.[22]

4.5 Laser Cavity Solitons

SMCs can also be generated in a nested laser cavity in which a Kerr microresonator is embedded into a gain fiber cavity.[21] The principle of laser cavity soliton is demonstrated in Fig. 18(a), which includes a microring cavity and a longer gain fiber cavity. The mode relationship of these two cavities is shown in Fig. 18(b), which ensures only a single fiber cavity mode in each microcavity mode to prevent supermode instability. The phases of comb lines are locked based on the intracavity FWM effect,[90,91] and a typical optical spectrum of laser cavity soliton is presented in Fig. 18(c). The main gain of laser cavity soliton is obtained by stimulated radiation in the gain fiber cavity, which is different from the parametric gain of external-pumped microcomb generation schemes. Therefore, the intracavity power does not need to reach the OPO threshold, which results in laser cavity soliton formation with very low power.

Comparatively, the laser cavity soliton is background-free, which is beneficial for improving the energy conversion efficiency. According to the LLE, the energy conversion efficiency is limited to 5% for CW laser pumped single soliton. However, the conversion efficiency of laser cavity soliton can be boosted to 96% in

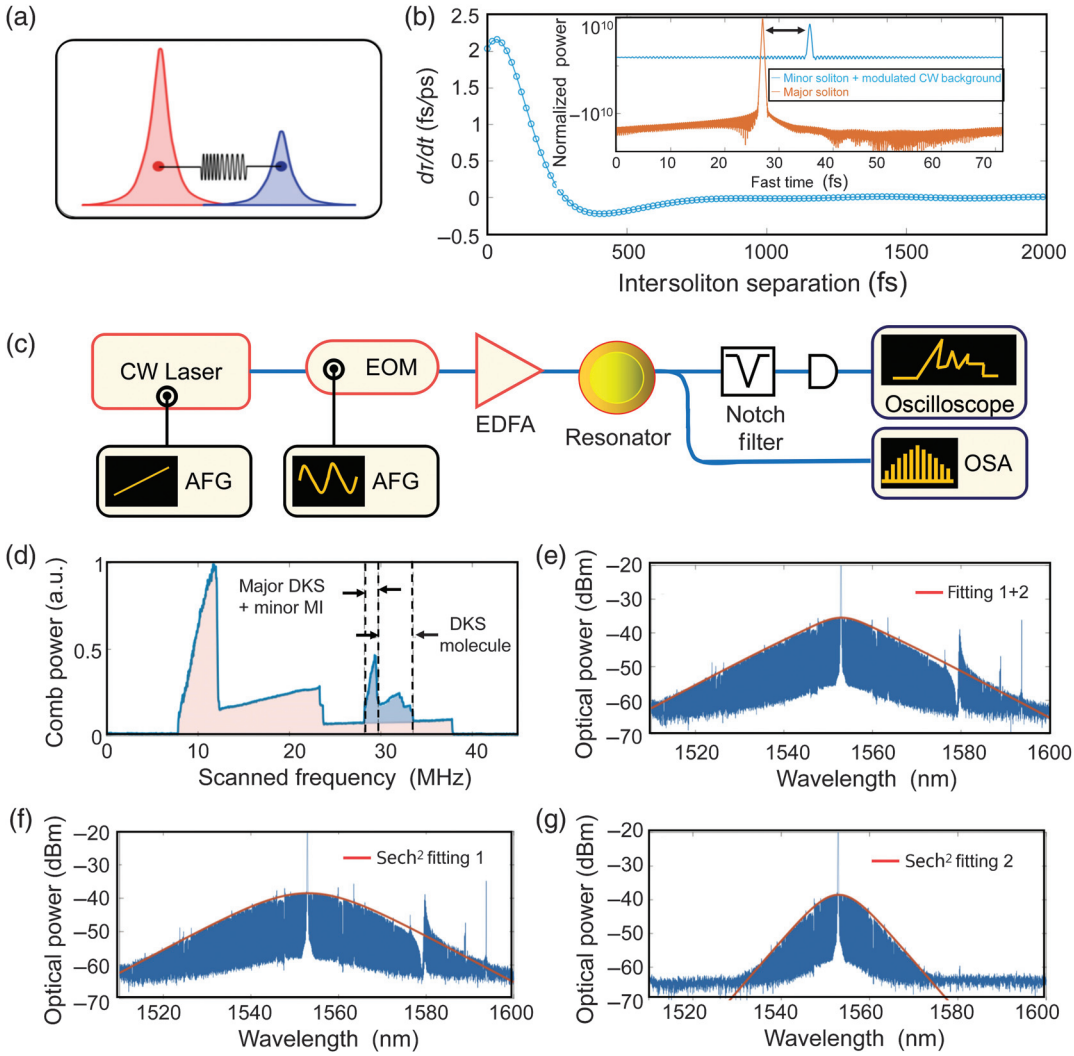

Fig. 17 Heteronuclear soliton molecule generation using two discrete pumps. (a) Principle of bound solitons where attractive force and repulsive force are balanced. (b) Calculated repulsive force versus the temporal separation of solitons. (c) The experimental setup for soliton molecule generation. (d) Measured transmission power trace while the pumps sweep across a cavity resonance. The red-shaded area is the comb power of the major pump, while the comb power of the minor pump is indicated by the blue-shaded area. (e) Optical spectrum of soliton molecules of two bound solitons, which corresponds to a linear superposition of optical spectra of the major soliton (f) and minor soliton (g). Images are adapted with permission from Ref. 22.

theory, and 75% is experimentally obtained.[21] Furthermore, as the lasing modes are the common modes of nested cavities, the repetition rate of cavity soliton can be simply tuned through changing the fiber cavity length (e.g., using a high-precision delay line), providing a new approach for the realization of SMC frequency locking. Meanwhile, the generation of laser cavity solitons mainly relies on the modes relationship of nested cavities, so they exhibit high robustness against environment fluctuations.

4.6 Dark Soliton Generation in the Normal-Dispersion Regime

Dark solitons (or dark pulses) are generally understood as intensity dips on a constant background, which demonstrate some unique advantages (e.g., less sensitivity to the system loss than bright solitons and more stability against the Gordon–Haus jitter in long communication lines) and have attracted increasing interest in many areas. Based on the mean-field LLE in the context of ring cavities or Fabry–Pérot interferometer with transverse spatial extent, it is found that in the time domain the dark solitons manifest themselves as low-intensity dips embedded in a high-intensity homogeneous background with a complex temporal structure, as being a particular type of solitons appearing in dissipative systems.[92,93] Although the original nonlinear Schrödinger equation admits a solution in the form of bright solitons in the anomalous-dispersion regime, dark solitons are in the normal-dispersion regime.[94,95] It is worth noting that mode-locking transitions do not necessarily correspond to dark or bright pulse (soliton) generation in microresontors with normal dispersion.[96,97] This is in contrast to the situations for the

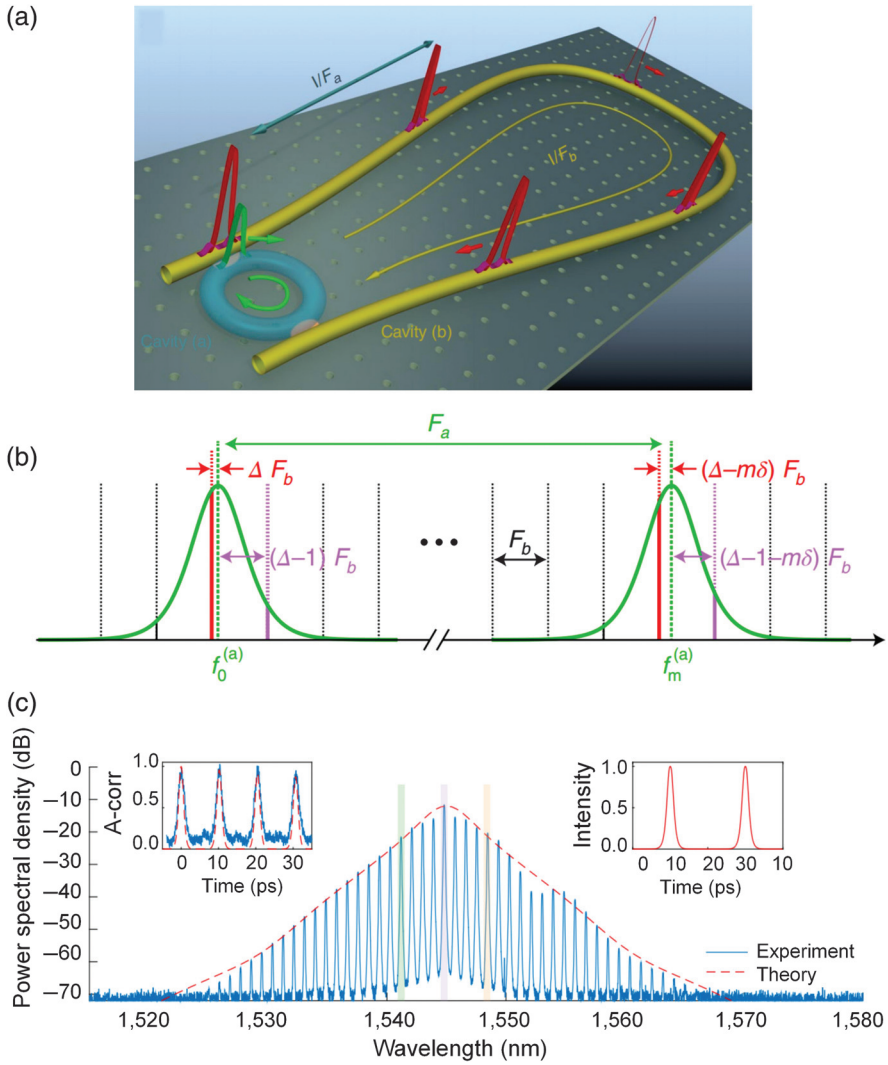

Fig. 18 Laser cavity solitons. (a) Principle of cavity soliton formation. The microresonator is nested into a gain fiber cavity. (b) Mode relationship of the nonlinear microresonator and gain fiber cavity. (c) Typical optical spectrum of laser cavity soliton, which includes two equidistant solitons per round-trip. Images are adapted with permission from Ref. 21.

negative-dispersion regime where all soliton forms are actually "bright solitons." Actually, in the field of traditional mode-locked fiber lasers, it has been proved that different types of bright pulses can emit from a laser cavity in the normal-dispersion regime, including dissipative solitons with rectangular spectrum (Gaussian in time domain), Gaussian spectrum (flat-topped pulses), broadband spectrum (wave-breaking-free pulses), and noise-like pulses (low-coherence pulse clusters).[98] Or even, bright and dark solitons can coexist in the same fiber laser cavity with strong normal dispersion.[94] A similar phenomenon is also theoretically revealed in normal-dispersion microresonators.[95] In other words, it can be considered that there does not exist a rigid "barrier" to distinguish the two states (depending on the pulse duration and duty cycle). Since rich phenomena have been discovered exhibiting distinct features from different aspects and with rather complicated excitation dynamics, there have been various prediction and explanations related to the physical origin of the observed temporal behaviors for microcombs with normal dispersion in the literature, such as "platicons" (flat-topped bright solitonic pulses),[99] dark pulses,[23,92] and dark solitons[93,95,96] or just normal-dispersion microcombs.[97] In this part, we mainly focus on the mode-locked character, rather than a strict physical clarification for this kind of pulse. For simplicity, these localized reduction structures with an intense CW background in microcavites are all referred to as "dark solitons."

An obvious difference between the two opposite-dispersion regimes is that the anomalous region usually favors ultrashort pulse emission with time-bandwidth-product limited (chirp-free or nearly chirp-free) durations, while for the normal-dispersion regime it prefers strongly chirped waves that are far from the Fourier-transform limitation with the absence of intrinsic balancing between the nonlinearity and negative dispersion. Thus intuitively, the route to DS generation as well as its excitation dynamics will deviate from those for bright solitons in anomalous-dispersion microresonators. During the past years, several experiments with normal-dispersion resonators on diverse material platforms, including CaF_2[100] and MgF_2 WGM

resonators,[101] as well as SiN microrings,[97,102] emerged. Numerous trials regarding different skills concerning the microcomb formation were also conducted. For instance, as shown in Figs. 19(a) and 19(b), by utilizing backscattered light from a resonator to lock the laser to the WGM microresonator (self-injection locking method),[100] a stable DS state corresponding to a manifold of short "dark" pulses with lower power compared to the background traveling inside the resonator is achieved, and the phase-locked comb shows three distinct maxima (peaks) on the spectrum envelope.[101] Through numerical analysis, it is found that the position of these peaks depends on the normalized dispersion value, which is similar to the situations for the negative dispersion where the comb bandwidth and the position of the emitted dispersive wave are decided by the overall dispersion. Another example using a SiN microring is depicted in Fig. 19(c).[102] The system is driven from the hyperparametric oscillation that is facilitated by the local dispersion disruptions induced by mode interactions to a mode-locked DS state over a 200-nm spectral bandwidth at a selected pump power and detuning. Interestingly, it is found that even square

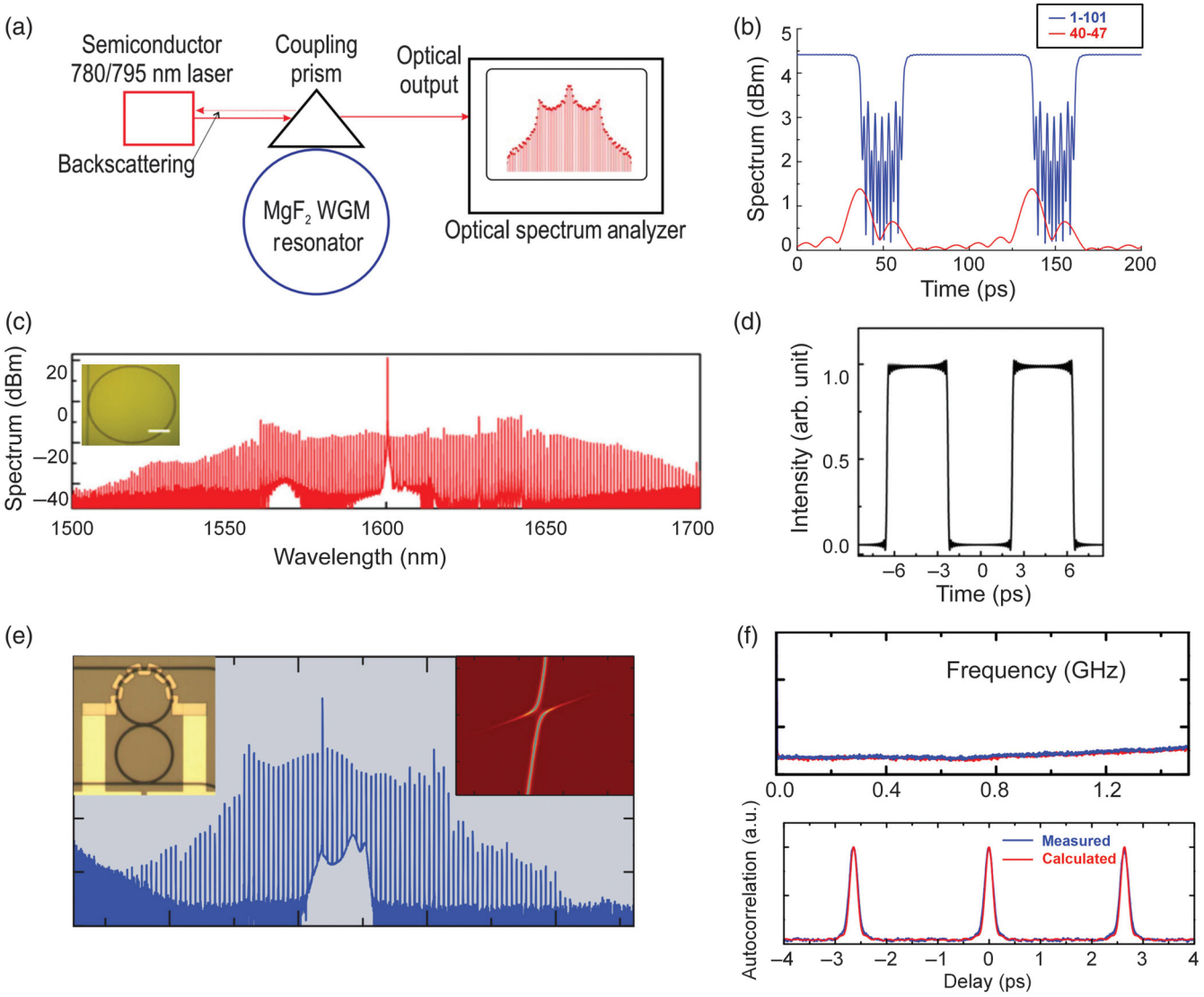

Fig. 19 Frequency comb generation in normal-dispersion microcavities. (a) Experiment setup using a semiconductor laser self-injection locked to an MgF_2 WGM resonator, wherein the spectral envelope shows three distinct maxima. (b) Numerically simulated envelope of intracavity optical pulses in terms of normalized amplitude (blue) and the pulse formed by only a limited number of modes with no pump frequency included (red).[101] (c) Example comb spectrum spanning more than 200 nm obtained in a SiN microring (inset: an optical micrograph of the microring). (d) Square optical pulses directly generated under special conditions at high pump power.[102] (e) Spectrum for the mode-locked state using dual-coupled SiN microrings in normal-dispersion regime.[97] Insets: microscope image of microrings (upper left) and transmission spectra versus heater power showing the resonances can be selectively split (upper right). (f) Comb intensity noise corresponding to (e) measurement by an electrical spectrum analyzer (top) and autocorrelation of the transform-limited pulse after line-by-line shaping (bottom).

pulses can be generated directly with correct sets of wavelength-dependent Q-factor, GVD, and pump detuning [Fig. 19(d)].[102] Other achievements in this field include using a dual-coupled microresonator integrated with an on-chip microheater to shift the auxiliary ring resonances via the thermo-optic effect, as shown in Figs. 19(e) and 19(f), thus permitting programmable and reliable control of mode interactions that help the comb initially generated at specified resonances to achieve repetition-rate selectable and mode-locked combs in the normal-dispersion regime.[97] Furthermore, it has also been numerically proved that the third-order dispersion plays an important role in the existence and stability of dark solitons, even allowing for stable dark and bright solitons to coexist in a microcavity.[95]

All of this progress demonstrates that the mode-locking mechanism for normal-dispersion microcavities might have analogies to, but surely is not identical to, that in anomalous-dispersion regimes. One of the most obvious differences, compared with bright solitons observed in negative-dispersion microcavities, is that the soliton regime now favors the blue-detuned region instead of the red-shifted regime, which leads to the intracavity pump field staying on the upper branch of the bistability curve where modulational instability is generally absent.[103,104] A representative work is shown in Figs. 20(a) and 20(b); a thermal-tuning method (equivalent to the traditional frequency tuning method) is employed to realize dark solitons in a SiN microring.[23] The pump is gradually tuned to stably approach the resonance from the blue side (and always in the effectively blue-detuned regime with respect to the shifted resonance); the power transmission curve is depicted in Fig. 20(a) and different operation stages are observed in Fig. 20(b). Strikingly, it can be clearly seen that the MI process, which is commonly cited as an important mechanism for SMC generation in the negative-dispersion regime, is now weakened (or even disappears) in this positive-dispersion regime. This mechanism is further verified by a detailed bifurcation analysis of dark structures in the LLE with normal GVD, which predicts DS regions of existence and stability, and it suggests that the MI does not play a role in the DS existence.[92] By contrast, mode coupling, which is usually considered to be detrimental as it inhibits the formation of solitons and limits the comb bandwidth in the anomalous-dispersion cavities, now acts as a contributing factor for initiation of DS generation.[23,103] It is suggested that the initial comb lines are formed due to the interaction of different mode families; if resonances corresponding to different families of transverse modes approach each other in frequency, they may interact around mode crossing positions.[23,104] This principle is also supported in a related work using the second-harmonic-assisted approach for DS generation in which the interaction between the fundamental and second-harmonic waves can provide a new way of phase matching for FWM in optical microresonators, effectively enabling the DS generation [Fig. 20(c)].[104] One more interesting phenomenon is that, as shown in Figs. 20(d)

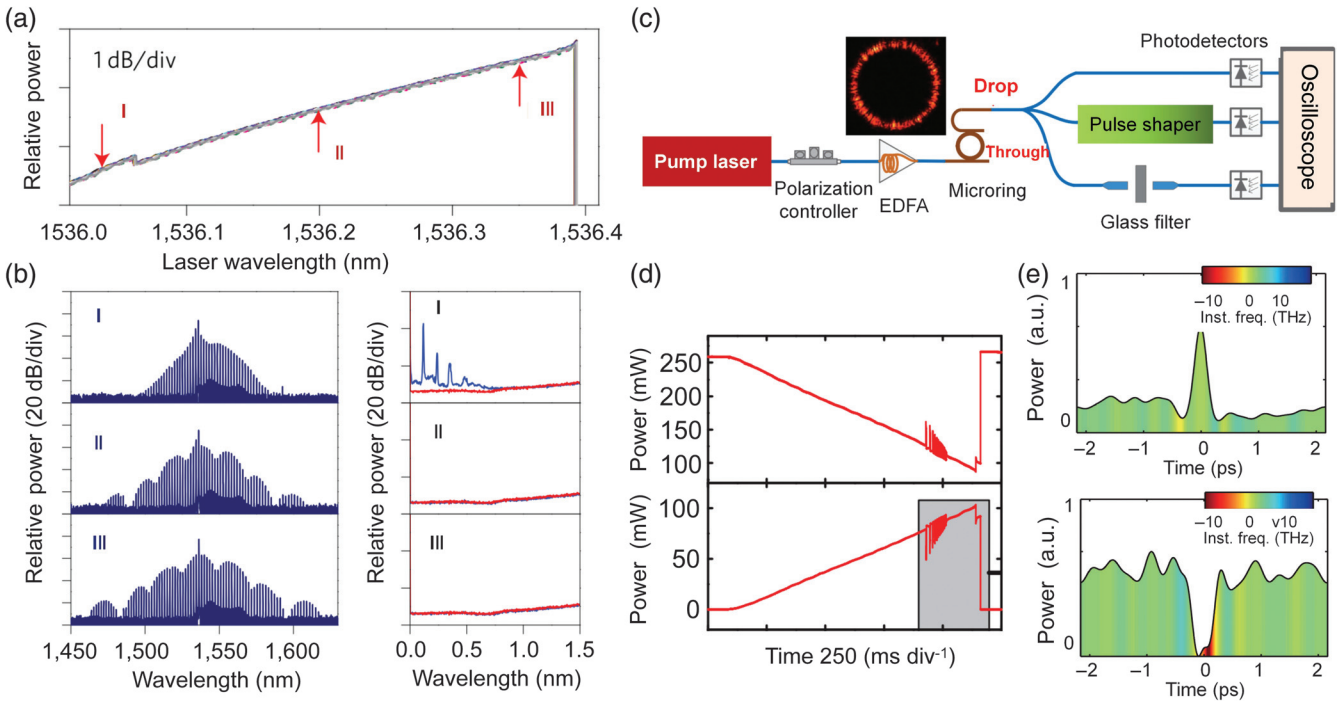

Fig. 20 DS generation in a normal-dispersion SiN microring using (a) and (b) the thermal-tuning method[23] and (c)–(e) second-harmonic-assisted approach.[93] (a) Drop-port power transmission when one mode is pumped. (b) Comb spectra (left panel) and intensity noise (right panel) corresponding to different stages in (a). (c) Experimental setup for the second-harmonic-assisted comb generation. Inset: microscope image of the microring with second-harmonic radiation. (d) Transition curves of the through port (top) and drop port (bottom) when the pump laser scans across the resonance from shorter to longer wavelengths. (e) Reconstructed waveforms at through port (top) and drop port (bottom), showing bright and dark pulses, respectively (inst. freq.: instantaneous frequency). Images (a) and (b) are adapted with permission from Ref. 23 and images (c)–(e) are adapted with permission from Ref. 104.

and 20(e), at the through port bright solitons are observed, while at the drop port DSs are captured (i.e., they are reciprocal). Considering the physical nature, it is reasonable to imagine that the intracavity generation of bright pulses usually leads to generation of DSs at the output for the add-drop type microresonators. Moreover, with specific operation parameters, it is possible to transform the cavity state from the bright soliton regime to the DS state or vice versa.[92] Therefore, the most important meaning of the DS research relies on such approaches providing a novel way of overcoming the dispersion limit for traditional microcombs. This is very important for effectively extending the accessible wavelength ranges, e.g., stretching to visible ranges that are essential for the stabilization of optical clocks where the atomic transitions locate but large normal material dispersion usually dominates.[23]

Looking back on the research of extraordinary SMCs related to rich physical phenomena (including soliton crystals, Stokes solitons, breathers, molecules, and cavity solitons, as well as dark solitons), all of these encouraging discoveries have revealed deeper insight into the dynamics and properties of this new category of laser sources for integrated photonics. As a comparison, the developing route is, interestingly and legitimately, mimicking the evolution roadmap of the mode-locked fiber lasers of previous pioneers in nonlinear optics in the last few decades (and still continuously yielding cutting-edge progresses at present[105]). Actually, a lot of unusual phenomena in microcombs have already been predicted or verified in a similar manner to some degree. That is, although different in material platforms and generation mechanisms, classic fiber nonlinearities can still offer a guidance or reference for microcombs, especially regarding unexplored temporal and spectral behaviors (e.g., vector solitons,[106,107] wave-breaking-free pulses,[108,109] optical bullets,[110] or even rouge waves[111,112]). Meanwhile, they can inspire new fundamental research on intrinsic soliton features that are not yet considered in this area, such as the chirp parameter (or time-bandwidth-product),[113] which is crucial in traditional fiber lasers for dedicated control on pulse shaping qualities[114] and contributes significantly to further system optimization.

5 Applications

To date, various proof-of-concept experiments concerning extensive applications of SMCs have been demonstrated (Fig. 21), including massively parallel coherent communications, DCS, ultrafast distance measurements, low-noise microwave generation, optical frequency synthesizers, astrophysical spectrometer calibration, and quantum information processing. Some representative works are discussed by classification of application fields.

5.1 Coherent Optical Communications

Future demand in "big data" interconnection leads to optical communication systems with terabits to petabits per second data rates in a single fiber with hundreds of parallel wavelength-division multiplexing channels. The SMC can act as a promising candidate of multiwavelength carriers due to its favorable characteristics of frequency stability, broad band, suitable mode spacing, and narrow linewidth. Even based on a nonsoliton-state microcomb with an imperfect spectrum, Pefeifle et al.[115] demonstrated coherent transmission of 1.44 Tbit/s of data over 300 km, using 20 comb channels with spectral efficiency of 3 bit/(s · Hz) under quadrature phase-shift keying modulating and polarization multiplexing. When SMCs were used, the data rate was successfully boosted to 55 Tbit/s with spectral efficiency of 5.2 bit/(s · Hz), under the conditions of 179 channels, 50 GHz carrier spacing, 40 gigabaud rate, 16-state quadrature amplitude modulation (16-QAM), and 75-km transmitting distance.[39] Higher order modulation of 64-QAM has also been achieved by employing dark SMCs.[116] A record high spectral efficiency of up to 10 bit/(s · Hz) was recently realized using the traditional superchannel method.[117]

5.2 Spectroscopy

The DCS, which is similar to Fourier transform spectroscopy, provides an excellent method for gas composition detection with outstanding features of shorter sampling time, higher optical spectrum resolution, and multicomposition detection capability. Two SMCs in the telecommunication band with slightly different repetition rates that were generated in two separate SiO_2 wedge disk resonators were used to build a DCS system, and the absorption spectrum of $H^{13}CN$ was analyzed.[38] An improved approach utilizing counter-propagating solitons emitted from a single cavity was reported recently to implement a Vernier spectrometer, which provided a considerable technical simplification. The Vernier spectrometer enhanced the capability for arbitrarily tuned source measurement.[118] High-performance dual-soliton-combs using two cascaded SiN microresonators with a single pump, which drastically reduces experimental complexity, have also been demonstrated.[119] In the mid-infrared region, molecular transitions are much higher (typically 10 to 1000 times) than that in the visible or near-IR, and a proof-of-principle mid-infrared DCS system based on silicon microrings was successfully realized through a thermal-controlled method.[120] In addition to the DCS, single- and triple-SMCs have also been proposed for atomic spectroscopy and multidimensional coherent spectroscopy, respectively.[80,121]

5.3 Distance Measurement

OFCs are promising as excellent coherent sources for light detection and ranging (LIDAR) systems to fulfill fast and accurate distance measurements. Using a setup similar to the DCS system, dual-comb ranging systems have been carried out recently, which opens the door to low-SWaP LIDAR systems. For example, by employing the dual counter-propagating SMCs within a single silica wedge resonator, a dual-comb laser ranging system substantiates the time-of-flight measurement with 200-nm accuracy at an averaging time of 500 ms and within a range ambiguity of 16 mm.[65] Another parallel progress is achieved on a SiN dual-microcomb LIDAR system, demonstrating ultrafast distance measurements with a precision of 12 nm at averaging times of 13 μs and acquisition rates of 100 MHz, even allowing for in-flight sampling of gun projectiles moving as fast as 150 m/s.[41] Through fast chirping pump lasers in the soliton existence range, the pump frequency modulation was transferred to all spectral comb lines, which resulted in a true parallelism frequency-modulated continuous-wave LIDAR.[122] SMC was also proposed for high-accuracy, long distance ranging based on a dispersive interferometry method. In a very recent experiment, a minimum Allan deviation of 27 nm was successfully achieved in an outdoor 1179 m ranging experiment.[123]

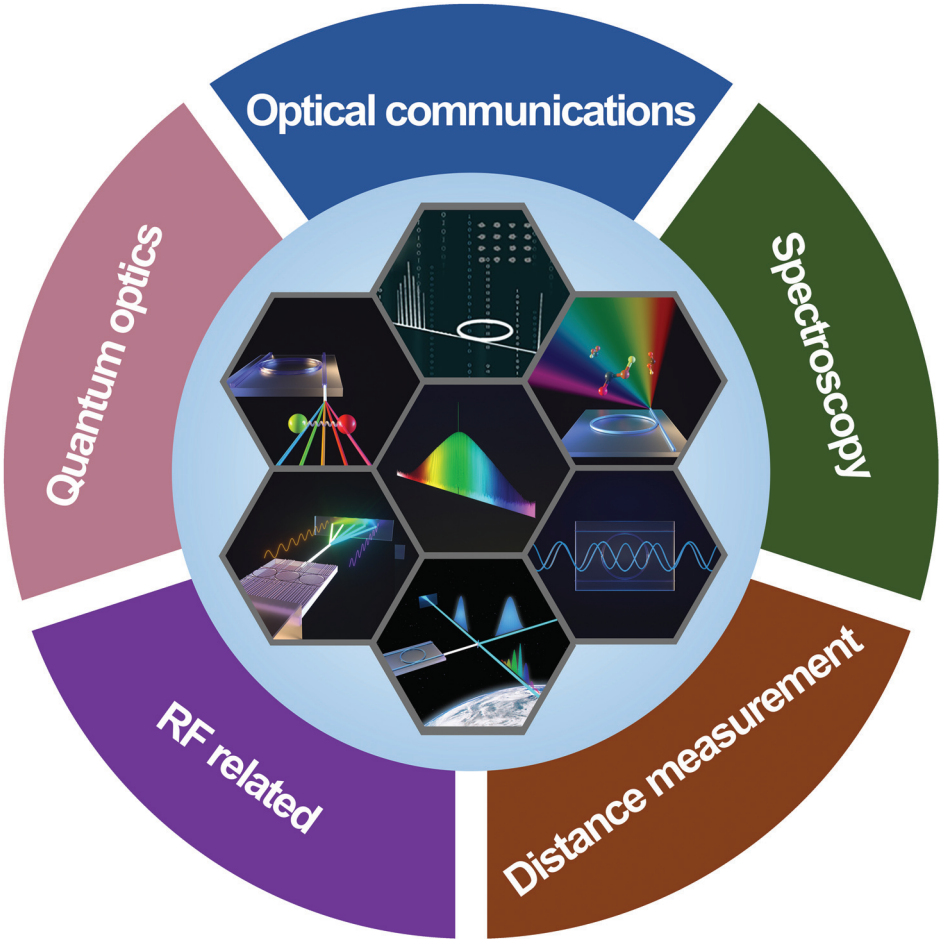

Fig. 21 Application areas of SMCs.

5.4 RF Related

SMCs are promising candidates for microwave-related applications including optical atomic clocks, ultrastable microwave generation, and microwave signal processing. Early attempts of photonic-microwave links include locking a nonsoliton state microcomb to atomic Rb transitions[124] and a self-referenced microcomb with a broadened spectrum locked to an atomic clock.[125] Recently, more compact schemes with fully stabilized SMCs have been reported, taking a big step toward photonic integration of optical-frequency synthesis[40,126] and optical atomic clocks.[127] The proposed optical frequency synthesizer was verified to be capable of transferring the stability from a 10-MHz microwave clock to laser frequency within an uncertainty of $\leq 7.7 \times 10^{-15}$.[40] An updated work demonstrated that with the help of a pair of interlocked SMCs, an optical atomic clock can provide fully coherent optical division to generate a 22-GHz RF clock signal with a fractional frequency instability of 10^{-13}.[128] In addition to the photonic-microwave link, SMCs can also act as important tools for high spectral purity microwave generation[129,130] and true time delays.[131–135]

5.5 Quantum Optics

Benefitting from the significant cavity enhancement, microresonators can offer attractive integrated platforms for single photon or entangled quantum state generation.[136] Broadband quantum frequency comb has been realized in a high-refractive-index glass microring resonator via a high-efficiency spontaneous FWM effect at a relatively low pump power.[137] Based on the quantum microcomb technique, more breakthroughs have been achieved, including the first integrated multiphoton entanglement[137] and high-dimensional entangled quantum states.[138] Compared with the quantum microcomb relying on the spontaneous parametric process, SMCs generated through the stimulated FWM effect can also play important roles in quantum optics. For example, a novel quantum key distribution system by demultiplexing the coherent microcomb lines was proposed very recently, showing the potential of the Gbps secret key rate.[139] Considering other progress made in this field by utilizing microcombs,[140–146] it is reasonable to imagine that the microcavities can find more important applications worth extensively exploring in quantum optics.

6 Summary and Outlook

The experimental realization of SMCs represents the successful convergence of materials science, physics, and engineering techniques. SMCs have been regarded as an outstanding candidate in the exploration of next generation of optical sources due to the unprecedented advantages of lower SWaP (size,

weight, and power), higher repetition rate as well as high coherence across the spectral coverage.[147] Until now, the challenge of SMC generation has been gradually overcome using a variety of advanced experimental techniques, from the universal power-kicking method to the "forward and backward tuning" scheme for deterministic single SMC generation. Meanwhile, the dynamics of cavity soliton physics are substantially understood along with discovery of various extraordinary solitons and the rich nonlinear effects of dispersive waves, mode-crossing effect, and Raman self-frequency shift.

Although SMC-based applications present unprecedented performance improvements in many fields, generally they are still at the stage of proof-of-concept in laboratories at present. Considering engineering applications, the developments of SMCs (should) favor the tendency toward automatic generation, as well as higher integration density and higher energy conversion efficiency. The main challenge of automatic or programmable-controlled SMC generation comes from the ultrashort thermal lifetime of a microresonator, which is beyond the capacity of practical instruments for timely judgment on the soliton state through spectrum recognition. Fortunately, some advanced tuning speed independent schemes (e.g., the auxiliary-laser-assistant method and photorefractive effect in $LiNbO_3$ microresonators) have been raised, paving a potential way for automatic SMC generation. Monolithic/hybrid integration is another key technique to promote applications of SMCs. The core issue of fully integrated SMC sources is improving the Q-factor of microresonators. The propagation loss in microcavities is still several orders of magnitude higher than that of standard optical fibers, so there is still great potential to further lower the loss through optimizing the fabrication process. Actually, many achievements have been obtained via improved microfabrication techniques. For example, environmentally stable silicon oxynitride (SiO_xN_y) with a Q even higher than 100 million (two orders higher than the previous level) has been successfully realized; it permits a submicrowatt threshold for microcomb generation[148–150]. In addition, hybrid-integrated SMC sources through butt-coupling gain block or LD to SiN chips have been reported recently.[52,72] Furthermore, higher energy conversion efficiency[151,152] of SMC sources is demanded for reducing power consumption. Currently, researchers are purchasing higher conversion efficiency through different routes, including the self-injection method,[33] perfect soliton crystals,[83] dark pulse,[23] and coupled-ring geometry,[91] as well as nearly 100% via a pump recycling method.[152]

It should be noted that a majority of reported SMCs are operating at communication bands. However, there are still great challenges for the generation of visible and mid-infrared SMCs, which would enable broad applications in molecular spectroscopy and chemical/biological sensing. The bandwidth of visible SMC[28] is rather limited, and no mid-infrared single-SMC has yet been reported. Therefore, more efforts to improve the performance of SMCs on existing platforms and explore new materials are expected for vastly extending the spectral coverage to reach their full potential.[153,154] Furthermore, microcavities are yet to be thoroughly developed and recognized by revealing more characteristics in the space and time domains, so as to identify their intrinsic essences and ultimate capabilities.[155–158] Considering all of these breakthroughs, it is highly likely that SMCs will become revolutionary integrated optical sources with ultralow SWaP in a wide range of future applications.

Acknowledgments

This work was supported by the National Natural Science Foundation of China (Grant Nos. 61635013 and 61675231), the Strategic Priority Research Program of the Chinese Academy of Sciences (Grant No. XDB24030600), and the Youth Innovation Promotion Association of CAS (Grant No. 2016353). The authors thank Z. Z. Lu, X. Y. Wang, and B. L. Zhao for valuable discussions and contributions to document proofreading.

References

1. K. J. Vahala, "Optical microcavities," *Nature* **424**, 839–846 (2003).
2. T. J. Kippenberg, S. M. Spillane, and K. J. Vahala, "Kerr-nonlinearity optical parametric oscillation in an ultrahigh-Q toroid microcavity," *Phys. Rev. Lett.* **93**, 083904 (2004).
3. A. A. Savchenkov et al., "Low threshold optical oscillations in a whispering gallery mode CaF_2 resonator," *Phys. Rev. Lett.* **93**, 243905 (2004).
4. M.-G. Suh and K. Vahala, "Gigahertz-repetition-rate soliton microcombs," *Optica* **5**, 65–66 (2018).
5. W. Q. Wang et al., "Dual-pump Kerr micro-cavity optical frequency comb with varying FSR spacing," *Sci. Rep.* **6**, 28501 (2016).
6. T. J. Kippenberg, R. Holzwarth, and S. A. Diddams, "Microresonator-based optical frequency combs," *Science* **332**(6029), 555–559 (2011).
7. D. K. Armani et al., "Ultra-high-Q toroid microcavity on a chip," *Nature* **421**, 925–928 (2003).
8. P. Del'Haye et al., "Optical frequency comb generation from a monolithic microresonator," *Nature* **450**, 1214–1217 (2007).
9. Y. Okawachi et al., "Octave-spanning frequency comb generation in a silicon nitride chip," *Opt. Lett.* **36**(17), 3398–3400 (2011).
10. T. Herr et al., "Temporal solitons in optical microresonators," *Nat. Photonics* **8**, 145–152 (2014).
11. D. C. Cole et al., "Kerr-microresonator solitons from a chirped background," *Optica* **5**, 1304–1310 (2018).
12. V. Brasch et al., "Photonic chip-based optical frequency comb using soliton Cherenkov radiation," *Science* **351**(6271), 357–360 (2016).
13. X. Yi et al., "Soliton frequency comb at microwave rates in a high-Q silica microresonator," *Optica* **2**, 1078–1085 (2015).
14. C. Joshi et al., "Thermally controlled comb generation and soliton modelocking in microresonators," *Opt. Lett.* **41**(11), 2565–2568 (2016).
15. Z. Lu et al., "Deterministic generation and switching of dissipative Kerr soliton in a thermally controlled micro-resonator," *AIP Adv.* **9**, 025314 (2019).
16. H. Zhou et al., "Soliton bursts and deterministic dissipative Kerr soliton generation in auxiliary-assisted microcavities," *Light Sci. Appl.* **8**, 50 (2019).
17. Q.-F. Yang et al., "Stokes solitons in optical microcavities," *Nat. Phys.* **13**, 53–57 (2017).
18. Q.-F. Yang et al., "Counter-propagating solitons in microresonators," *Nat. Photonics* **11**, 560–564 (2017).
19. W. Q. Wang et al., "Robust soliton crystals in a thermally controlled microresonator," *Opt. Lett.* **43**(9), 2002–2005 (2018).
20. C. Bao et al., "Observation of Fermi–Pasta–Ulam recurrence induced by breather solitons in an optical microresonator," *Phys. Rev. Lett.* **117**, 163901 (2016).
21. H. Bao et al., "Laser cavity-soliton microcombs," *Nat. Photonics* **13**, 384–389 (2019).
22. W. Weng et al., "Heteronuclear soliton molecules in optical microresonators," arXiv: 1901-04026v1.
23. X. Xue et al., "Mode-locked dark pulse Kerr combs in normal-dispersion microresonators," *Nat. Photonics* **9**, 594–600 (2015).
24. T. Herr et al., "Mode spectrum and temporal soliton formation in optical microresonators," *Phys. Rev. Lett.* **113**, 123901 (2014).

25. M. Karpov et al., "Raman self-frequency shift of dissipative Kerr solitons in an optical microresonator," *Phys. Rev. Lett.* **116**, 103902 (2016).
26. X. Yi et al., "Single-mode dispersive waves and soliton microcomb dynamics," *Nat. Commun.* **8**, 14869 (2017).
27. Z. Lu et al., "Raman self-frequency-shift of soliton crystal in a high index doped silica micro-ring resonator," *Opt. Mater. Express* **8**, 2662–2669 (2018).
28. R. Niu et al., "Repetition rate tuning of soliton in microrod resonators," arXiv:1809.06490 (2018).
29. S. Y. Zhang et al., "Sub-milliwatt-level microresonator solitons with extended access range using an auxiliary laser," *Optica* **6**, 206–212 (2019).
30. Z. Gong et al., "High-fidelity cavity soliton generation in crystalline AlN micro-ring resonators," *Opt. Lett.* **43**(18), 4366–4369 (2018).
31. Y. He et al., "Self-starting bi-chromatic $LiNbO_3$ soliton microcomb," *Optica* **6**, 1138–1144 (2019).
32. M. Yu et al., "Mode-locked mid-infrared frequency combs in a silicon microresonator," *Optica* **3**, 854–860 (2016).
33. S. H. Lee et al., "Towards visible soliton microcomb generation," *Nat. Commun.* **8**, 1295 (2017).
34. M. H. P. Pfeiffer et al., "Octave-spanning dissipative Kerr soliton frequency combs in Si_3N_4 microresonators," *Optica* **4**, 684–691 (2017).
35. M. Karpov et al., "Photonic chip-based soliton frequency combs covering the biological imaging window," *Nat. Commun.* **9**, 1146 (2018).
36. I. S. Grudinin et al., "High-contrast Kerr frequency combs," *Optica* **4**, 434–437 (2017).
37. P.-H. Wang et al., "Intracavity characterization of micro-comb generation in the single-soliton regime," *Opt. Express* **24**(10), 10890–10897 (2016).
38. M. Suh et al., "Microresonator soliton dual-comb spectroscopy," *Science* **354**(6312), 600–603 (2016).
39. P. Marin-Palomo et al., "Microresonator-based solitons for massively parallel coherent optical communications," *Nature* **546**, 274–279 (2017).
40. D. T. Spencer et al., "An optical-frequency synthesizer using integrated photonics," *Nature* **557**, 81–85 (2018).
41. P. Trocha et al., "Ultrafast optical ranging using microresonator soliton frequency combs," *Science* **359**(6378), 887–891 (2018).
42. M.-G. Suh et al., "Searching for exoplanets using a microresonator astrocomb," *Nat. Photonics* **13**, 25–30 (2019).
43. A. Pasquazi et al., "Micro-combs: a novel generation of optical sources," *Phys. Rep.* **729**, 1–81 (2018).
44. L. Gaeta, M. Lipson, and T. J. Kippenberg, "Photonic-chip-based frequency combs," *Nat. Photonics* **13**, 158–169 (2019).
45. N. G. Pavlov et al., "Narrow-linewidth lasing and soliton Kerr microcombs with ordinary laser diodes," *Nat. Photonics* **12**, 694–698 (2018).
46. D. C. Cole et al., "Soliton crystals in Kerr resonaotors," *Nat. Photonics* **11**, 671–676 (2017).
47. J. R. Stone et al., "Thermal and nonlinear dissipative-soliton dynamics in Kerr-microresonator frequency combs," *Phys. Rev. Lett.* **121**, 063902 (2018).
48. Q. Li et al., "Stably accessing octave-spanning microresonator frequency combs in the soliton regime," *Optica* **4**, 193–203 (2017).
49. C. Bao et al., "Direct soliton generation in microresonators," *Opt. Lett.* **42**(13), 2519–2522 (2017).
50. Y. Geng et al., "Terabit optical OFDM superchannel transmission via coherent carriers of a hybrid chip-scale soliton frequency comb," *Opt. Lett.* **43**(10), 2406–2409 (2018).
51. M. Yu et al., "Breather soliton dynamics in microresonators," *Nat. Commun.* **8**, 14569 (2017).
52. B. Stern et al., "Battery-operated integrated frequency comb generator," *Nature* **562**, 401–405 (2018).
53. J. Liu et al., "Ultralow-power chip-based SMCs for photonic integration," *Optica* **5**, 1347–1353 (2018)
54. B. Yao et al., "Gate-tunable frequency combs in graphene-nitride microresonators," *Nature* **558**, 410–414 (2018).
55. Z. Gong et al., "Soliton microcomb generation at 2 μm in z-cut lithium niobate microring resonators," *Opt. Lett.* **44**(12), 3182–3185 (2019).
56. Y. K. Chembo and N. Yu, "Modal expansion approach to optical frequency-comb generation with monolithic whispering gallery-mode resonators," *Phys. Rev. A* **82**, 033801 (2010).
57. Y. K. Chembo and N. Yu, "On the generation of octave-spanning optical frequency combs using monolithic whispering-gallery-mode microresonators," *Opt. Lett.* **35**(16), 2696–2698 (2010).
58. A. B. Matsko et al., "Mode-locked Kerr frequency combs," *Opt. Lett.* **36**(15), 2845–2847 (2011).
59. Y. K. Chembo and C. R. Menyuk, "Spatiotemporal Lugiato–Lefever formalism for Kerr-comb generation in whispering-gallerymode resonators," *Phys. Rev. A* **87**, 053852 (2013).
60. S. Coen et al., "Modeling of octave-spanning Kerr frequency combs using a generalized mean-field Lugiato–Lefever model," *Opt. Lett.* **38**(1), 37–39 (2013).
61. T. Carmon, L. Yang, and K. J. Vahala, "Dynamical thermal behavior and thermal self-stability of microcavities," *Opt. Express* **12**(20), 4742–4750 (2004).
62. V. B. Braginsky, M. L. Gorodetsky, and V. S. Ilchenko, "Quality factor and nonlinear properties of optical whispering-gallery modes," *Phys. Lett. A* **137**, 393–397 (1989).
63. V. Brasch et al., "Bringing short-lived dissipative Kerr soliton states in microresonators into a steady state," *Opt. Express* **24**(25), 29312–29320 (2016).
64. X. Yi et al., "Active capture and stabilization of temporal solitons in microresonators," *Opt. Lett.* **41**(9), 2037–2040 (2016).
65. M.-G. Suh and K. J. Vahala, "Soliton microcomb range measurement," *Science* **359**(6378), 884–887 (2018).
66. Y. Geng et al., "Kerr frequency comb dynamics circumventing cavity thermal behavior," in *Nonlinear Opt.*, p. NM1A.4 (2017).
67. S. Zhang, J. Silver, and P. Del'Haye, "Spectral extension and synchronisation of microcombs in a single microresonator," arXiv: 2002.06168v1 (2020).
68. X. Guo et al., "Efficient generation of a near-visible frequency comb via Cherenkov-like radiation from a Kerr microcomb," *Phys. Rev. Appl.* **10**, 014012 (2018).
69. H. Guo et al., "Universal dynamics and deterministic switching of dissipative Kerr solitons in optical microresonators," *Nat. Phys.* **13**, 94–102 (2017).
70. V. V. Vassiliev et al., "Narrow-line-width diode laser with a high-Q microsphere resonator," *Opt. Commun.* **158**, 305–312 (1998).
71. N. M. Kondratiev et al., "Self-injection locking of a laser diode to a high-Q WGM microresonator," *Opt. Express* **25**(23), 28167–28178 (2017).
72. A. S. Raja et al., "Electrically pumped photonic integrated soliton microcomb," *Nat. Commun.* **10**, 680 (2019).
73. M.-G. Suh et al., "Directly pumped 10 GHz microcomb modules from low-power diode lasers," *Opt. Lett.* **44**(7), 1841–1843 (2019).
74. B. Shen et al., "Integrated turnkey soliton microcombs operated at CMOS frequencies," arXiv:1911.02636v1 (2019).
75. A. S. Voloshin et al., "Dynamics of soliton self-injection locking in a photonic chip-based microresonator," arXiv:1912.11303v2 (2020).
76. E. Obrzud, S. Lecomte, and T. Herr, "Temporal solitons in microresonators driven by optical pulses," *Nat. Photonics* **11**, 600–607 (2017).
77. E. Obrzud et al., "A microphotonic astrocomb," *Nat. Photonics* **13**, 31–35 (2019).
78. F. Leo et al., "Temporal cavity solitons in one-dimensional Kerr media as bits in an all-optical buffer," *Nat. Photonics* **4**, 471–476 (2010).
79. M. Pang et al., "All-optical bit storage in a fibre laser by optomechanically bound states of solitons," *Nat. Photonics* **10**, 454–458 (2016).

80. L. Stern et al., "Direct Kerr frequency comb atomic spectroscopy and stabilization," *Sci. Adv.* **6**, eaax6230 (2020).
81. B. L. Zhao et al., "Repetition-rate multiplicable soliton microcomb generation and stabilization via phase-modulated pumping scheme," *Appl. Phys. Express* **13**, 032009 (2020).
82. M. Karpov et al., "Dynamics of soliton crystals in optical microresonators," *Nat. Phys.* **15**, 1071–1077 (2019).
83. Y. He et al., "Perfect soliton crystals on demand," arXiv: 1910.00114v1 (2019).
84. K. Y. Yang et al., "Broadband dispersion-engineered microresonator on-a-chip," *Nat. Photonics* **10**, 316–320 (2016).
85. H. Guo et al., "Intermode breather solitons in optical microresonators," *Phys. Rev. X* **7**, 041055 (2017).
86. C. J. Bao et al., "Effect of a breather soliton in Kerr frequency combs on optical communication systems," *Opt. Lett.* **41**(8), 1764–1767 (2016).
87. A. B. Matsko, A. A. Savchenkov, and L. Maleki, "On excitation of breather solitons in an optical microresonator," *Opt. Lett.* **37**(23), 4856–4858 (2012).
88. E. Lucas et al., "Breathing dissipative solitons in optical microresonators," *Nat. Commun.* **8**, 736 (2017).
89. B. Kibler et al., "The Peregrine soliton in nonlinear fibre optics," *Nat. Phys.* **6**, 790–795 (2010).
90. M. Peccianti et al., "Demonstration of a stable ultrafast laser based on a nonlinear microcavity," *Nat. Commun.* **3**, 765 (2012).
91. W. Wang et al., "Repetition rate multiplication pulsed laser source based on a microring resonator," *ACS Photonics.* **4**, 1677–1683 (2017).
92. P. P. Rivas et al., "Origin and stability of dark pulse Kerr combs in normal dispersion resonators," *Opt. Lett.* **41**(11), 2402–2405 (2016)
93. P. P. Rivas et al., "Dark solitons in the Lugiato–Lefever equation with normal dispersion," *Phys. Rev. A* **93**, 063839 (2016).
94. L. R. Wang, "Coexistence and evolution of bright pulses and dark solitons in a fiber laser," *Opt. Commun.* **297**, 129–132 (2013).
95. P. P. Rivas, D. Gomila, and L. Gelens, "Coexistence of stable dark- and bright-soliton Kerr combs in normal-dispersion resonators," *Phys. Rev. A* **95**, 053863 (2017).
96. X. H. Hu et al., "Spatiotemporal evolution of continuous-wave field and dark soliton formation in a microcavity with normal dispersion," *Chin. Phys. B* **26**, 074216 (2017).
97. X. X. Xue et al., "Normal-dispersion microcombs enabled by controllable mode interactions," *Laser and Photonic Rev.* **9**, L23–L28 (2015).
98. L. R. Wang et al., "Observations of four types of pulses in a fiber laser with large net-normal dispersion," *Opt. Express* **19**(8), 7616–7624 (2011).
99. V. E. Lobanov, G. Lihachev, and M. L. Gorodetsky, "Generation of platicons and frequency combs in optical microresonators with normal GVD by modulated pump," *Europhys. Lett.* **112**, 54008 (2015).
100. A. A. Savchenkov et al., "Tunable optical frequency comb with a crystalline whispering gallery mode resonator," *Phys. Rev. Lett.* **101**, 093902 (2008).
101. W. Liang et al., "Generation of a coherent near-infrared Kerr frequency comb in a monolithic microresonator with normal GVD," *Opt. Lett.* **39**(10), 2920–2923 (2014).
102. S. W. Huang et al., "Mode-locked ultrashort pulse generation from on-chip normal dispersion microresonators," *Phys. Rev. Lett.* **114**, 053901 (2015).
103. Y. Liu et al., "Investigation of mode coupling in normal-dispersion silicon nitride microresonators for Kerr frequency comb generation," *Optica* **2**, 137–144 (2014).
104. X. X. Xue et al., "Second-harmonic assisted four-wave mixing in chip-based microresonator frequency comb generation," *Light Sci. Appl.* **6**, e16253 (2017).
105. Z.-X. Ding et al., "All-fiber ultrafast laser generating gigahertz-rate pulses based on a hybrid plasmonic microfiber resonator," *Adv. Photon.* **2**(2), 026002 (2020).
106. H. Zhang et al., "Coherent energy exchange between components of a vector soliton in fiber lasers," *Opt. Express* **16**(17), 12618–12623 (2008).
107. Y. Xiang et al., "Scalar and vector solitons in a bidirectional mode-locked fibre laser," *J. Lightwave Technol.* **37**, 5108–5114 (2019).
108. D. Mao et al., "Partially polarized wave-breaking-free dissipative soliton with super-broad spectrum in a mode-locked fiber laser," *Laser Phys. Lett.* **8**(2), 134–138 (2011).
109. N. Akhmediev and A. Ankiewicz, *Dissipative Solitons*, Lecture Notes in Physics, Vol. **661**, Springer-Verlag, Berlin, Heidelberg (2005).
110. G. Fibich and B. Ilan, "Optical light bullets in a pure Kerr medium," *Opt. Lett.* **29**(8), 887–889 (2004)
111. M. Tlidi et al., "Drifting cavity solitons and dissipative rogue waves induced by time-delayed feedback in Kerr optical frequency comb and in all fiber cavities," *Chaos* **27**, 114312 (2017).
112. Y. F. Song et al., "Recent progress on optical rogue waves in fiber lasers: status, challenges, and perspectives," *Adv. Photon.* **2**(2), 024001 (2020).
113. L. R. Wang, X. M. Liu, and Y. K. Gong, "Giant-chirp oscillator for ultra-large net-normal dispersion fiber lasers," *Laser Phys. Lett.* **7** (1), 63–67 (2010).
114. L. R. Wang et al., "Dissipative soliton generation/compression in a compact all-fibre laser system," *Electron. Lett.* **47**(6), 392–393 (2011).
115. J. Pfeifle et al., "Coherent terabit communications with microresonator Kerr frequency combs," *Nat. Photonics* **8**, 375–380 (2014).
116. A. Fülöp et al., "High-order coherent communications using mode-locked dark-pulse Kerr combs from microresonators," *Nat. Commun.* **9**, 1598 (2018).
117. M. Mazur et al., "Enabling high spectral efficiency coherent super channel transmission with SMCs," arXiv: 1812.11046 (2018).
118. Q. Yang et al., "Vernier spectrometer using counter-propagating SMCs," *Science* **363**(6430), 965–968 (2019).
119. A. Dutt et al., "On-chip dual-comb source for spectroscopy," *Sci. Adv.* **4**, e1701858 (2018).
120. M. Yu et al., "Silicon-chip-based mid-infrared dual-comb spectroscopy," *Nat. Commun.* **9**, 1869 (2018).
121. E. Lucas et al., "Spatial multiplexing of soliton microcombs," *Nat. Photonics* **12**, 699–705 (2018).
122. J. Riemensberger et al., "Massively parallel coherent laser ranging using soliton microcombs," arXiv:1912.11374v1 (2019).
123. J. Wang et al., "Long distance measurement using single soliton microcomb," arXiv:2002.10565 (2020).
124. S. B. Papp et al., "Microresonator frequency comb optical clock," *Optica* **2**, 10–14 (2014).
125. P. Del'Haye et al., "Phase-coherent microwave-to-optical link with a self-referenced microcomb," *Nat. Photonics* **10**, 516–520 (2016).
126. S.-W. Huang et al., "A broadband chip-scale optical frequency synthesizer at 2.7×10^{-16} relative uncertainty," *Sci. Adv.* **2**, e1501489 (2016).
127. Z. L. Newman et al., "Architecture for the photonic integration of an optical atomic clock," *Optica* **6**, 680–685 (2019).
128. F. Alishahi et al., "Reconfigurable optical generation of nine Nyquist WDM channels with sinc-shaped temporal pulse trains using a single microresonator-based Kerr frequency comb," *Opt. Lett.* **44**(7), 1852–1855 (2019).
129. W. Liang et al., "High spectral purity Kerr frequency comb radio frequency photonic oscillator," *Nat. Commun.* **6**, 7957 (2015).
130. W. Weng et al., "Spectral purification of microwave signals with disciplined dissipative Kerr solitons," *Phys. Rev. Lett.* **122**, 013902 (2019).
131. X. Xu et al., "Advanced RF and microwave functions based on an integrated optical frequency comb source," *Opt. Express* **26**(3), 2569–2583 (2018).

132. X. Xu et al., "An optical micro-comb with a 50-GHz free spectral range for photonic microwave true time delays," arXiv:1711.03927 (2017).
133. X. Y. Xu et al., "Reconfigurable broadband microwave photonic intensity differentiator based on an integrated optical frequency comb source," *APL Photonics* **2**(9), 096104 (2017).
134. X. X. Xue and A. M. Weiner, "Microwave photonics connected with microresonator frequency combs," *Front. Optoelectron.* **9**, 238–248 (2016).
135. X. X. Xue et al., "Microresonator frequency combs for integrated microwave photonics," *IEEE Photonics Technol. Lett.* **30**, 1814–1817 (2018).
136. M. Kues et al., "Quantum optical microcombs," *Nat. Photonics* **13**, 170–179 (2019).
137. C. Reimer et al., "Generation of multiphoton entangled quantum states by means of integrated frequency combs," *Science* **351**(6278), 1176–1180 (2016).
138. M. Kues et al., "On-chip generation of high-dimensional entangled quantum states and their coherent control," *Nature* **546**, 622–626 (2017).
139. F.-X. Wang et al., "Quantum key distribution with on-chip dissipative Kerr soliton," *Laser Photon. Rev.* **14**, 1900190 (2020).
140. L. Caspani et al., "Multifrequency sources of quantum correlated photon pairs on-chip: a path toward integrated quantum frequency combs," *Nanophotonics* **5**(2), 351–362 (2016).
141. C. L. Xiong, B. Bell, and B. J. Eggleton, "CMOS-compatible photonic devices for single-photon generation," *Nanophotonics* **5**(3), 427–439 (2016).
142. C. Reimer et al., "CMOS-compatible, multiplexed source of heralded photon pairs: towards integrated quantum combs," *Opt. Express* **22**(6), 6535–6546 (2014).
143. W. C. Jiang et al., "Silicon-chip source of bright photon pairs," *Opt. Express* **23**(16), 20884–20904 (2015).
144. R. Wakabayashi et al., "Time-bin entangled photon pair generation from Si micro-ring resonator," *Opt. Express* **23**(2), 1103–1113 (2015).
145. D. Grassani et al., "Micrometer-scale integrated silicon source of time-energy entangled photons," *Optica* **2**, 88–94 (2015).
146. P. Imany et al., "50-GHz-spaced comb of high-dimensional frequency-bin entangled photons from an on-chip silicon nitride microresonator," *Opt. Express* **26**(2), 1825–1840 (2018).
147. T. J. Kippenberg et al., "Dissipative Kerr solitons in optical microresonators," *Science* **361**(6402), eaan8083 (2018).
148. D. Chen et al., "On-chip ultra-high-Q silicon oxynitride optical resonators," *ACS Photonics* **4**, 2376–2381 (2017).
149. D. Chen et al., "Normal dispersion silicon oxynitride microresonator Kerr frequency combs," *Appl. Phys. Lett.* **115**, 051105 (2019).
150. A. Kovach et al., "Emerging material systems for integrated optical Kerr frequency combs," *Adv. Opt. Photonics* **12**, 135–222 (2020).
151. B. Y. Kim et al., "Turn-key, high-efficiency Kerr comb source," *Opt. Lett.* **44**(18), 4475–4478 (2019).
152. X. X. Xue, X. P. Zheng, and B. K. Zhou, "Super-efficient temporal solitons in mutually coupled optical cavities," *Nat. Photonics* **13**, 616–622 (2019).
153. L. R. Wang et al., "Frequency comb generation in the green using silicon nitride microresonators," *Laser Photonics Rev.* **10**, 631–638 (2016).
154. M. Zhang et al., "Broadband electro-optic frequency comb generation in a lithium niobate microring resonator," *Nature* **568**, 373–377 (2019).
155. J. G. Zhu et al., "On-chip single nanoparticle detection and sizing by mode splitting in an ultrahigh-Q microresonator," *Nat. Photon.* **4**, 46–49 (2010).
156. B.-Q. Shen et al., "Detection of single nanoparticles using the dissipative interaction in a high-Q microcavity," *Phys. Rev. Appl.* **5**, 024011 (2016).
157. D. Xu et al., "Synchronization and temporal nonreciprocity of optical microresonators via spontaneous symmetry breaking," *Adv. Photon.* **2**(4), 046002 (2019).
158. J. Liu et al., "Photonic microwave generation in the X- and K-band using integrated soliton microcombs," *Nat. Photon.* (2020).

Weiqiang Wang is an associate professor at the State Key Laboratory of Transient Optics and Photonics of Xi'an Institute of Optics and Precision Mechanics (XIOPM) of the Chinese Academy of Sciences (CAS). His research has focused on planar waveguide and devices, semiconductor lasers, Kerr optical frequency comb, and related applications.

Leiran Wang received his PhD from the University of CAS in 2011. At present, he is a professor at the State Key Laboratory of Transient Optics and Photonics of XIOPM and at the School of Future Technology of the University of CAS. His current research interests include integrated photonics and ultrafast nonlinear optics.

Wenfu Zhang is a professor at the State Key Laboratory of Transient Optics and Photonics of XIOPM of CAS and at the School of Future Technology of the University of CAS. His research interests focus on integrated photonics, nonlinear optics, and microstructure devices.